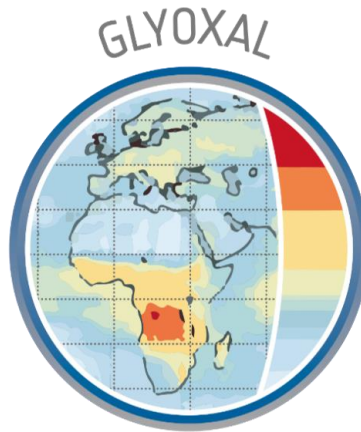


GLYoxal Retrievals from TROPOMI (GLYRETRO)

S5p+I - Validation Report (VR)



Prepared by:

Christophe Lerot

Royal Belgian Institute for Space Aeronomy

Leonardo Alvarado and Andreas Richter

Institute of Environmental Physics, University of Bremen

document number : S5p+I_CHOCHO_BIRA_VR

issue : 2.1

date : 2021-12-22

status : Final

Table of Contents

1.	Purpose and objective	3
2.	References, Acronyms and Abbreviations	3
2.1.	References	3
2.2.	Acronyms and abbreviations	4
3.	Product requirements	5
4.	Reference measurements	6
4.1.	Ground based monitoring network	6
4.2.	Satellite measurements and Modelling support.....	7
5.	Validation approach	8
5.1.	Comparison with ground-based measurements.	9
5.1.1.	Revisiting the glyoxal retrieval from ground-based data	9
5.1.2.	Results from validation using ground-based data	15
5.1.3.	Dependence on influence quantities	22
5.1.4.	Bias and short term variability	23
5.1.5.	Status of validation	24
5.2.	Inter-satellite comparison.	24
5.1.6.	TROPOMI inter-algorithm comparison.....	24
5.1.7.	Inter-sensor comparison	33
6.	Conclusions	41
7.	References	43

1. Purpose and objective

The purpose of this document is to describe the validation operations of the CHOCHO S5P+I Level-2 product. This report includes details of all validation activities performed based on ground-based data as well as on data from other satellite sensors, description of their settings and main differences to GLYRETRO.

2. References, Acronyms and Abbreviations

2.1. References

[RDO1] Sentinel-5 Level-2 Prototype Processor Development Requirements Specification;

source: ESA; **ref:** S5-RS-ESA-GR-0131; **issue:** 1.7; **date:** 2018-06-29.

[RDO2] Copernicus Sentinels 4 and 5 Mission Requirements Traceability Document (MRTD):

source: ESA; **ref:** EOP-SM/2413/BV-bv; **issue:** 2.0 **date:** 2017-07-07.

[RDO3] Sentinel-4 L2 Processor Component Development–Project Management Plan, DLR, S4-L2-DLR-PMP-1004, issue 2.1, 2017-05-31.

[RDO4] S5L2PP: Record of agreements from negotiation;
source: S5L2PP proposal consortium; **ref:** ST-ESA-S5L2PP-NOT-003; **Issue:** 1.1; **date:** 2016-09-02.

2.2. Acronyms and abbreviations

AMF: Air mass factor

BIRA-IASB: Royal Belgian Institute for Space Aeronomy

CHOCHO: Glyoxal

CTM: Chemical Transport Model

GLYRETRO: GLYoxal Retrievals from TROPOMI

MAX-DOAS: Multi-Axis DOAS

IUP: Institute of Environmental Physics

OMI: Ozone Monitoring Instrument

S5P: Sentinel-5 Precursors

SCD: Slant Column Density

TROPOMI: Tropospheric Monitoring Instrument

VCD: Vertical Column Density

3. Product requirements

Requirements have been defined for a series of key species, including particulate matter, ozone, NO₂, CO, SO₂ and HCHO. Since it has been generally considered as a second priority, no requirement on the glyoxal column uncertainty has been defined in the S4/5 MRTD [RDo2]. For the requirements on horizontal resolution and revisit time, we can use those defined for the formaldehyde columns, as those two species are useful for similar applications. The spatial requirement for HCHO has been set to 5/20 km (goal/threshold) for air quality applications and relaxed to 10/50 km for climate applications. The revisit time requirement is 0.5/2 hours for air quality applications and can obviously not be met for space instruments boarded on LEO platforms such as TROPOMI. In comparison, the future Sentinel-4 instrument aboard a geostationary platform will provide a one-hour revisit time.

Unlike for TROPOMI, glyoxal is part of the initial list of core operational products for Sentinel-4 and -5. In this context, requirements on this product have also been defined [RDo1, RDo3, RDo4] and are given in Table 1. While one single total uncertainty requirement is defined for Sentinel-4, two separate values are defined for the random and systematic components of the uncertainty in Sentinel-5.

Table 1: Uncertainty Requirements on glyoxal column retrievals defined for the Sentinel-4 and -5 missions.

	Uncertainty (Threshold)	Conditions
Sentinel-4	7 x 10 ¹⁴ molec.cm ⁻² or 50% (least stringent)	SZA < 60° VZA < 60° cloud fraction < 20% VCD > 5 x 10 ¹⁴ molec.cm ⁻²
Sentinel-5	Random error: < 1.5 x 10 ¹⁵ molec.cm ⁻² Systematic error: < 2.5 x 10 ¹⁴ molec.cm ⁻² or 50% (least stringent)	SZA < 70° VZA < 70°

4. Reference measurements

4.1. Ground based monitoring network

Several data sets are used in this study as glyoxal reference. All the instruments for which data was available are listed in Table 4-1 with their respective locations. Those data sets are derived from MAX-DOAS measurements from the ground, which mainly provide tropospheric vertical column density and may offer a potential to gain information on the vertical distribution. Figure 4-1 shows the geographical distribution of these data sets, which are mainly located over Europe and Asia.

Table 4-1: Independent MAX-DOAS measurements used in the validation of GLYRETRO.

Id	Location	Measurement Period	Type	Data Provider
Xi	Xianghe (China)	2008-present	MAX-DOAS	BIRA-IASB
Mo	Mohali (India)	2018-present	MAX-DOAS	MPIC/IISERM
Br	Bremen (Germany)	2014-present	MAX-DOAS	IUP-Bremen
Ath	Athens (Greece)	2018-present	MAX-DOAS	IUP-Bremen
Vi	Vienna (Austria)	2018-present	MAX-DOAS	IUP-Bremen
Chi	Chiba (Japan)	2018-present	MAX-DOAS	CEReS * http://atmos3.cr.chiba-u.jp/skynet/
Pant	Pantnagar (India)	2017-present	MAX-DOAS	CEReS * http://atmos3.cr.chiba-u.jp/skynet/
Phi	Phimai (Thailand)	2015-present	MAX-DOAS	CEReS * http://atmos3.cr.chiba-u.jp/skynet/

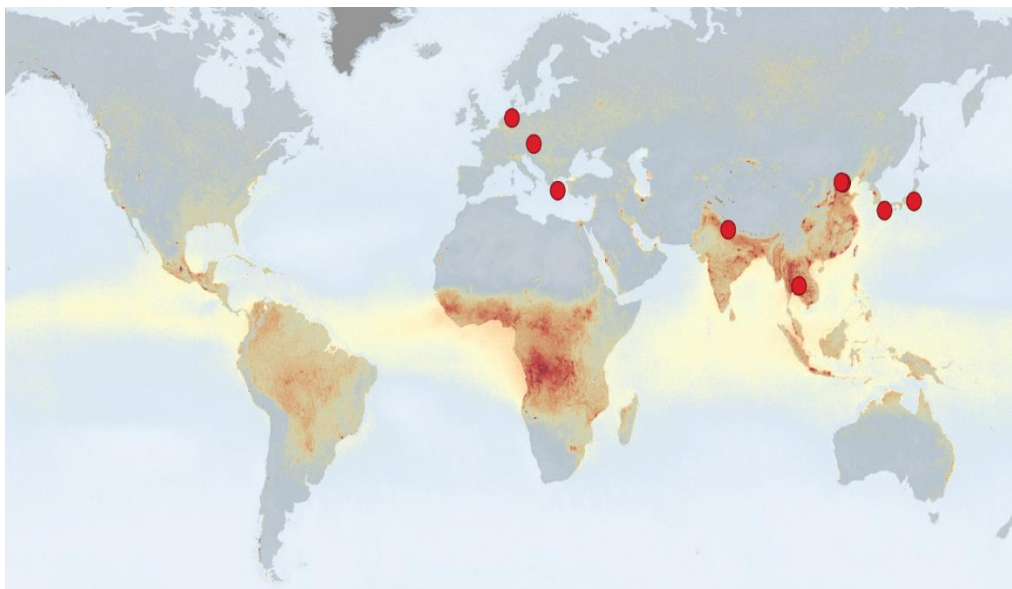


Figure 4-1: S5p Glyoxal global map retrieved using the GLYRETRO with the geographical locations of the MAX-DOAS measurements over Europe and Asia used in the validation.

4.2. Satellite measurements and Modelling support

Inter-satellite comparisons of glyoxal products are also important to assess their consistency and to verify that they can be combined together for specific studies (e.g. long-term trend analysis). Two types of comparison are performed and provide complementary information:

- Comparisons with the BIRA-IASB glyoxal products from OMI, GOME-2A and GOME-2B generated with a similar algorithm as that applied to TROPOMI provide information on possible differences related to instrumental characteristics. The GOME-2A/B data sets have been actually produced within the operational environment of the EUMETSAT AC SAF (Valks et al., 2020), based on a similar algorithmic baseline. Producing such a record from GOME-2C in the same environment is not planned to date. Therefore, it would be beneficial to do so in another context to extend the early morning satellite time series.

- Comparison with the IUP-Bremen TROPOMI (Alvarado et al., 2014, 2020) product allows assessing the agreement at different steps of the algorithms (e.g. SCD, offset corrections, AMF, VCDs).

In addition, comparing the TROPOMI product with glyoxal columns simulated with a CTM in different regions worldwide may support the evaluation of the geophysical soundness of the generated TROPOMI product, even if differences are expected given the large uncertainties in our knowledge of the glyoxal production and destruction mechanisms.

5. Validation approach

The GLYRETRO algorithm for the retrieval of CHOCHO is defined by BIRA-IASB. This algorithm is tested by independent satellite and ground-based data sets based on retrievals in similar spectral regions. Both the GLYRETRO and the MAX-DOAS algorithms are based on the well-established DOAS method (Platt and Stutz, 2008) and inherit from more than a decade of ground based and satellite retrievals (Alvarado et al., 2019, 2014; Lerot et al., 2010; Vrekoussis et al., 2009, 2010; Sienreich et al., 2007, 2010; Wittrock et al., 2006). Like all current satellite glyoxal column retrievals, the GLYRETRO algorithm consists of three elementary steps:

- The spectral retrieval of slant column densities (SCD), which are the number density of an absorber integrated along the light path.
- As CHOCHO retrievals are known to suffer from offsets (satellite only), often a semi-empirical bias correction is applied, for example by subtracting CHOCHO columns from a region over the Pacific or over the Sahara where low CHOCHO values are expected. If necessary, this bias correction can also be combined with a destriping step.
- Calculation of air mass factors (AMF) in radiative transfer simulations to convert the retrieved SCD to vertical columns (VCD), which correspond to absorber

amounts integrated along the vertical and are independent of the light path. Optionally, this step also includes treatment of clouds.

All these steps have associated uncertainties that arise from the technical implementation of the algorithm, and from uncertainties on the parameters describing the atmospheric state. The uncertainties related to a priori data on the atmospheric state can be assessed by comparing the TROPOMI CHOCHO VCD with independent products from other satellite sensors (e.g. OMI, GOME-2) and from ground-based instruments. In the following, results of GLYRETRO glyoxal columns are compared against MAX-DOAS data as well as against other satellite and model data (MAGRITTE 2018). The investigation starts with a sensitivity study performed to select optimal retrieval settings for ground-based data. Subsequently a comparison with available MAX-DOAS data is performed for the full period of S5P satellite measurements available at the time of writing and finally a preliminary comparison against other satellite and MAGRITTE data is presented.

5.1. Comparison with ground-based measurements.

5.1.1. Revisiting the glyoxal retrieval from ground-based data

During the last two decades, many efforts have been taken to improve the retrieval of weak absorbers such as CHOCHO. However, the uncertainties are still large in comparison to strong absorbers such as NO₂. Various algorithms and definitions of parameters used in CHOCHO retrievals are still in use, sometimes showing consistent results but sometimes also exhibiting large differences, depending on the wavelength window, polynomial and cross-sections of interfering species included in the retrieval. Therefore, we briefly revisit the CHOCHO retrieval in order to find the optimal parameters, based on sensitivity studies as described below.

For this glyoxal sensitivity study, measurements performed in Athens were used. A systematic variation of parameters has been performed to find the optimal parameter set for CHOCHO. The parameters evaluated were the cross-sections included in the retrieval, the fitting window, and the polynomial degree.

Start wavelength: 410 nm to 440 nm.

End wavelength: 442 nm to 472 nm.

Cross-sections: CHOCHO (Volkamer et al., 2005; 296 K), NO₂ (Vandaele et al., 1998; 220 K and 294 K), O₄ (Thalman et al., 2013; 293 K), O₃ (Serduchenko et al., 2014), H₂O (Rothman et al., 2013), Ring calculated by SCIATRAN model (Vountas et al., 1998).

Number of polynomial coefficients: 3 to 6.

Every combination of parameters was applied to more than 30 measurements per day at two elevation angles (2° and 30°) and using the zenith measurement closest in time as reference spectrum. In order to compensate possible straylight effects, a constant intensity offset was applied.

Figure 5-1 shows the mean root mean square (RMS) obtained in the glyoxal retrievals computed for all possible combinations of start and end wavelengths for each combination of cross-sections and polynomial degrees. The mean RMS decreases with increasing number of cross-sections, however this decrease is more significant when stronger absorbers are included in the fit, the most significant reduction being achieved by adding water vapour especially for 2° elevation. In addition, including a high temperature NO₂ cross-section leads to a reduction of mean RMS, by accounting for the tropospheric NO₂ contribution in the region of study. In addition, a polynomial with 6 coefficients leads to lower RMS, however no significant difference is observed between the results for polynomial degree 5 and 6.

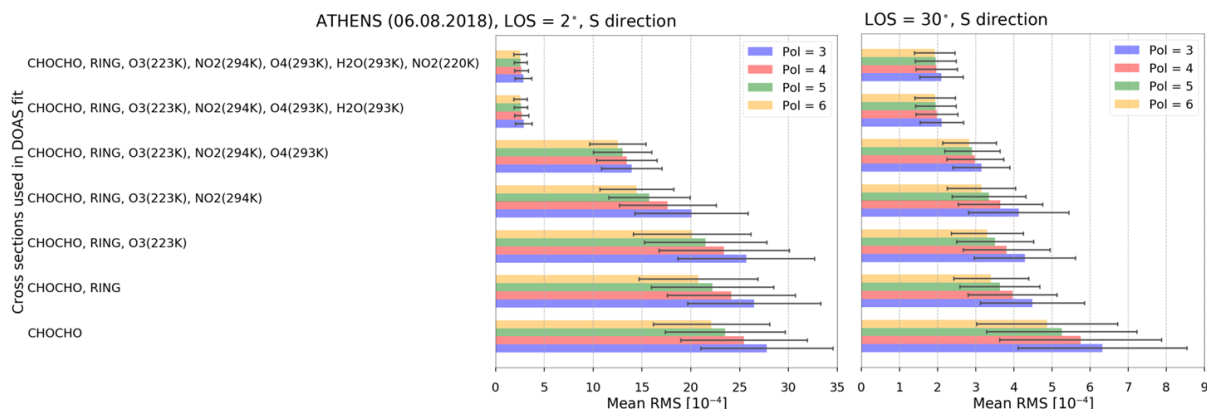


Figure 5-1: The mean RMS for glyoxal retrievals with their respective standard deviation as error bar computed over all possible fitting windows for each combination of cross-sections and different polynomials (colour bars) for measurements performed in Athens on 6 August 2018, elevation angle of 2° and 30° at an azimuth direction of 52.5° (S direction).

For the selection of fitting window, RMS, fit error, and SCD are evaluated as function of start and end limits of wavelength intervals at steps of 0.5 nm. These limits cover the most representative absorption bands of glyoxal. Figure 5-2 (a, b, c) shows the dependency of glyoxal retrievals on wavelength window for fit error, RMS and SCD at an elevation angle of 2° and azimuth viewing direction of 52.4° (S direction). Figure 5-2a shows the variability of fit error with wavelength, where red boxes denote the fit windows with lower fit errors; however regions that do not include the strongest absorption band of glyoxal are excluded. The lowest fit errors correspond to the interval with start wavelengths from 433 to 437.5 nm, and end wavelengths from 464 to 471 nm. This fit window is also within the intervals where the lower RMS is found (see Figure 5-2b, green boxes), the lowest RMS corresponding to intervals with start wavelengths from 433 to 440 nm and end wavelengths from 456 to 472 nm. For the SCDs some fit intervals show large variability (see Figure 5-2c, blue boxes). Only those fit windows with homogenous variability are selected and regions that do not contain the strongest absorption band of glyoxal are excluded. Thus, any fit window combination contained in the range with start wavelengths from 433 to 437.5 nm and end wavelengths from 464 to 472 is suitable for a good glyoxal retrieval considering the fact that these combinations also correspond to low

fit error and RMS. The lowest error corresponds to a fit window from 436 to 468 nm (polynomial with 6 coefficients).

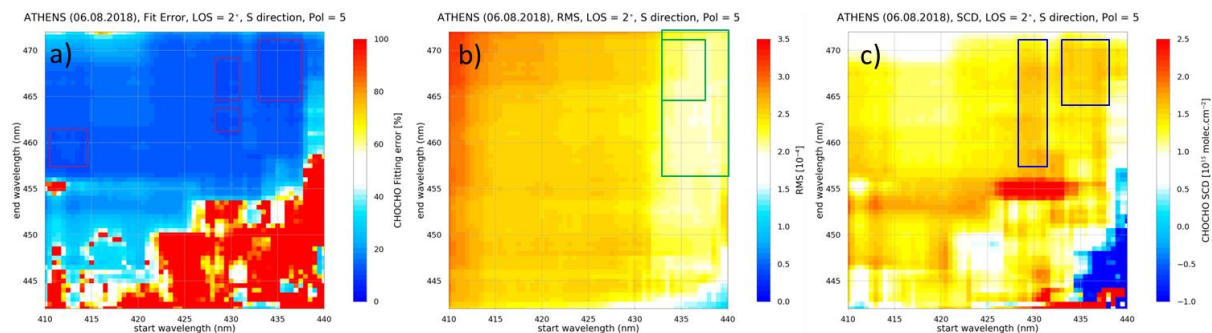


Figure 5-2: Colour mapping of a) fit errors, b) RMS, and c) SCD of CHOCHO for different wavelength windows with start limits of 410–440 nm and end limits of 442–472 nm for measurements performed at 2° elevation angle and an azimuth direction of 52.5° (S direction) over Athens on 6 August 2018.

In the following, retrievals using the parameters resulting from the sensitivity tests (Fit A) are compared to results obtained with the GLYRETRO (Fit C) and IUP S5P Glyoxal (Fit B) fit settings. These settings are summarized in the Table 5-1.

Figure 5-3 shows time series of CHOCHO SCD (a), fit error (b), and RMS (c) retrieved using three different settings (optimal – Fit A, IUP S5P Glyoxal – Fit B, GLYRETRO – Fit C). The SCDs are compared for elevation angles of 2° and 30°. The three retrievals show a similar temporal evolution with almost no difference among the SCDs. However, the retrieval using the optimal settings has the lowest error and an improvement of about 5% against the other two fits (see Figure 5-3b). A similar behaviour is observed in the comparison of RMS (see Figure 5-3c) but to a lesser degree.

Thus, this optimal fit will be applied to MAX-DOAS measurements performed in Athens, Vienna, Bremen, and Xianghe where the project participants are in charge of the instruments.

Table 5-1: DOAS settings for optimal retrieval (Fit A), IUP S5P (Fit B), and GLYRETRO (Fit C) applied to MAX-DOAS measurement from Athens.

Parameters	Fit A	Fit B	Fit C
Fitting window	436-468 nm	433-465 nm	435-460 nm
Polynomial	6 coefficients	5 coefficients	4 coefficients
Cross-sections used:			
CHOCHO (Volkamer et al., 2005)	Yes (296 K)	Yes (296 K)	Yes (296 K)
NO ₂ (Vandaele et al., 1998)	Yes (220, 294 K)	Yes (220, 294 K)	Yes (220, 294 K)
O ₄ (Thalman et al., 2013)	Yes (293 K)	Yes (293 K)	Yes (293 K)
O ₃ (Serduchenko et al., 2014)	Yes (223 K)	Yes (223 K)	Yes (223 K)
H ₂ O (Rothman et al., 2013)	Yes (296 K)	Yes (296 K)	Yes (296 K)
Ring effect	Ring cross section calculated by SCIATRAN model (Vountas et al., 1998)		

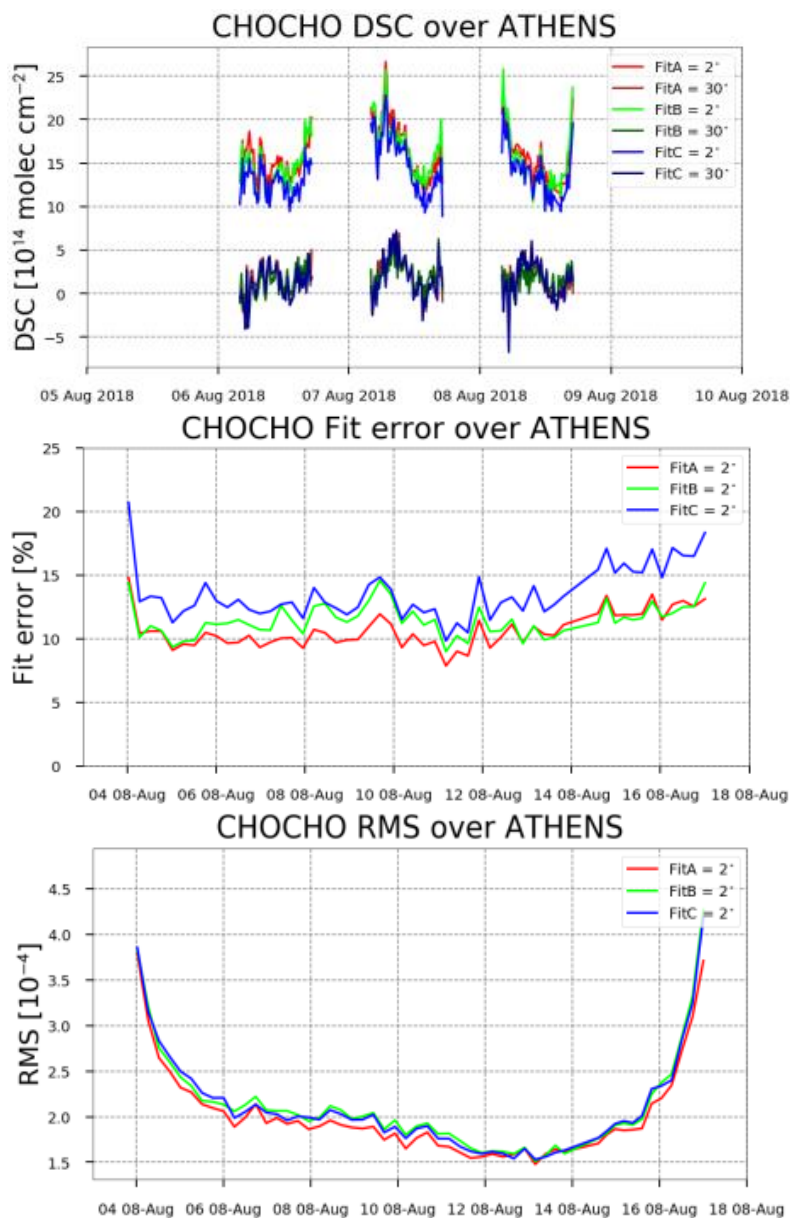


Figure 5-3: a) Time series of CHOCHO DSCs retrieved from the MAX-DOAS measurements in Athens at elevation angles of 2° and 30° with an azimuth direction of 52.5° (S direction) for the period between 6 and 9 August 2018. Also the fit error (b) and RMS (c) for 8 August 2018 presented.

5.1.2. Results from validation using ground-based data

In order to test the accuracy of GLYRETRO, glyoxal columns are compared to reference measurements acquired by Multi-Axis-DOAS measurements from stations located in Athens, Vienna, Bremen, Uccle, Xianghe, Pantnagar, Mohali, Chiba, and Phimai. Here, we collected an ensemble of data sets at nine stations located in Asia and Europe (see Table 4-1) spanning at least one year. Altogether, a wide range of glyoxal columns and emission regimes are covered by those stations. Unfortunately, current MAX-DOAS glyoxal retrievals are far from being homogenized, and can certainly not be considered as true fiducial reference measurements. For example, although the same interfering species (i.e. NO₂, water vapour, O₃, O₂-O₂, Ring) need to be included in the DOAS fits, the glyoxal differential slant columns may be retrieved in different fitting windows and with different reference cross-section data. Also, the design (spectral range, spectral resolution, detector type, etc) and operation mode of each instrument may differ substantially, resulting in different sensitivities to changes in retrieval settings. In addition, the slant-to-vertical column conversion is performed very differently from one station to another. Despite those limitations, the comparison of glyoxal tropospheric columns from satellites with nine different MAX-DOAS instruments is unprecedented.

Among the available MAX-DOAS data sets, three (Xianghe, Chiba and Phimai) are long enough to allow a comparison with OMI and GOME-2A/B in addition to TROPOMI. The other ones span shorter and more recent periods, and will only be used for comparison with the TROPOMI product. The Xianghe station is well controlled, processed for profiles using an optimal estimation scheme, and it has the longest data record. Therefore, it is used to perform a thorough analysis of the satellite product stability and of the impact of applying satellite averaging kernels. At the other stations, we focus on a more qualitative comparison of the seasonal cycles of the glyoxal tropospheric columns. For the data collocation, we select MAX-DOAS data ± 1.5 hour around the satellite overpass time and satellite data within a radius of 100 km (150 km for Phimai) and 20 km around the station for GOME-2A/B/OMI and TROPOMI, respectively. Daily median glyoxal columns are

computed if both satellite and ground-based data are available and finally monthly medians of the daily median columns are compared.

Figure 5-4 focuses on the comparison of monthly median glyoxal tropospheric columns retrieved from TROPOMI, OMI, GOME-2A and -2B with columns from the BIRA-IASB MAX-DOAS instrument in Xianghe (China). The left panels compare the full time series for each satellite sensor with the MAX-DOAS record. Right panels show the corresponding satellite/MAX-DOAS absolute differences. Note that the MAX-DOAS measurements have been interrupted from mid-2018 to mid-2019 due to an instrumental problem. Overall, all four satellite instruments reproduce quite well the seasonal cycle seen by the MAX-DOAS instrument. However, for all of them, except for the recent TROPOMI, a degradation appears after a few years of operation. For OMI, while the consistency with the MAX-DOAS is excellent before 2013, the number of outliers increases afterwards and the columns during wintertime become too low. The GOME-2A/B data sets also agree quite well with the ground-based data in their first years of operation but suffer from an increasing number of outliers after 2014 and 2017, respectively. Nonetheless, the quality of the data sets remain very reasonable. The consistency of the TROPOMI time series with the MAX-DOAS is also excellent and is characterized by a smooth temporal variability without any outliers on a monthly basis. The absolute differences shown in the right panels also clearly indicates a reduced scatter compared to the other satellites, despite the fact that a smaller overpass radius of 20 km was used instead of 100 km. This is reflected in the standard deviation of the differences given in the title of each subpanel. The TROPOMI standard deviation is 0.9×10^{14} molec/cm², while it is larger than 1.7×10^{14} molec/cm² for other sensors. On average, there are small negative biases with respect to the MAX-DOAS data for the four satellite time series (also given in the panel titles), ranging between -0.8×10^{14} molec/cm² for TROPOMI and 1.5×10^{14} molec/cm² for OMI.

For this particular station, we investigated the impact of applying the satellite averaging kernels to smooth the MAX-DOAS glyoxal profiles. This process allows simulating MAX-

DOAS columns, which would be retrieved from the satellite algorithm, considering its own a priori profile information. The comparison of the satellite columns with the smoothed MAX-DOAS data therefore removes differences due to imperfect satellite a priori profile information. As shown in Figure 5-4, smoothing the MAX-DOAS columns decreases them and reduces the satellite/MAX-DOAS bias to values ranging from -0.2×10^{14} molec/cm² (TROPOMI) to -0.5×10^{14} molec/cm² (OMI).

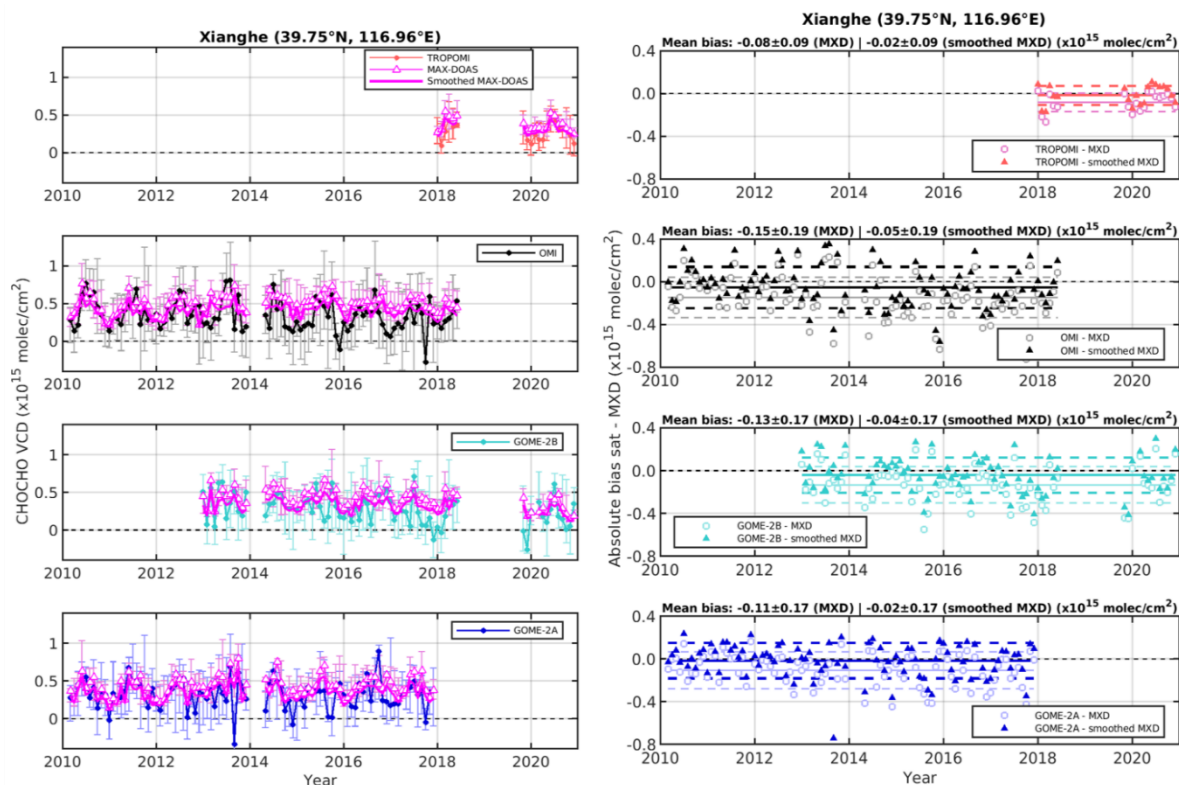


Figure 5-4: Comparison of the monthly median glyoxal tropospheric vertical columns retrieved from satellite and MAX-DOAS (MXD) instruments in Xianghe (China). The four left panels compare the time series from TROPOMI, OMI and GOME-2A/B with the MXD time series. MXD columns are also shown when smoothed with the satellite averaging kernels. The error bars represent the 25 and 75% percentiles. The four right panels show the corresponding time series of the satellite-MD absolute differences. Both original and smoothed MXD data are shown. Mean bias and standard deviation of the differences are given in the panel titles.

In Figure 5-5, we compare the median satellite and MAX-DOAS seasonal cycles of the glyoxal tropospheric columns at three stations (Xianghe, Chiba and Phimai) where the time series present a good overlap with the OMI and GOME-2A and B records, in addition to TROPOMI. In Xianghe, the seasonal cycle of the smoothed MAX-DOAS columns is also shown, illustrating again the reduction of the satellite/MAX-DOAS bias when the a priori profile error component is removed. Note that the OMI and GOME-2B seasonal cycles are computed using only data until end of 2013 and 2016, respectively to limit the impact of the increasing number of outliers. In each comparison panel, the MAX-DOAS cycle is always computed using the same time range as the satellite instrument. Overall, the seasonal patterns are consistently captured by the satellite and MAX-DOAS instruments. In Xianghe, the GOME-2A and TROPOMI cycles follow closely the MAX-DOAS curves, although TROPOMI slightly underestimates the MAX-DOAS columns during winter months. OMI and GOME-2B also reproduce the general seasonal pattern but show somewhat more scattered curves, likely due to their slightly less stable time series. In Chiba where the glyoxal signal is mostly driven by the biogenic cycle, the agreement between the satellites and the MAX-DOAS measurements is excellent both in terms of variability and absolute values. Again, OMI shows a more scattered curve (as also indicated by the larger error bars representing the inter-annual variability). In Phimai, where pyrogenic emissions are responsible for large glyoxal columns especially in the first few months of the year, the seasonal variability seen by the satellites and the MAX-DOAS is very consistent. However, a negative bias larger than for other stations is observed. This can be related to other studies that identified larger biases in NO₂ or HCHO DOAS products for elevated column conditions.

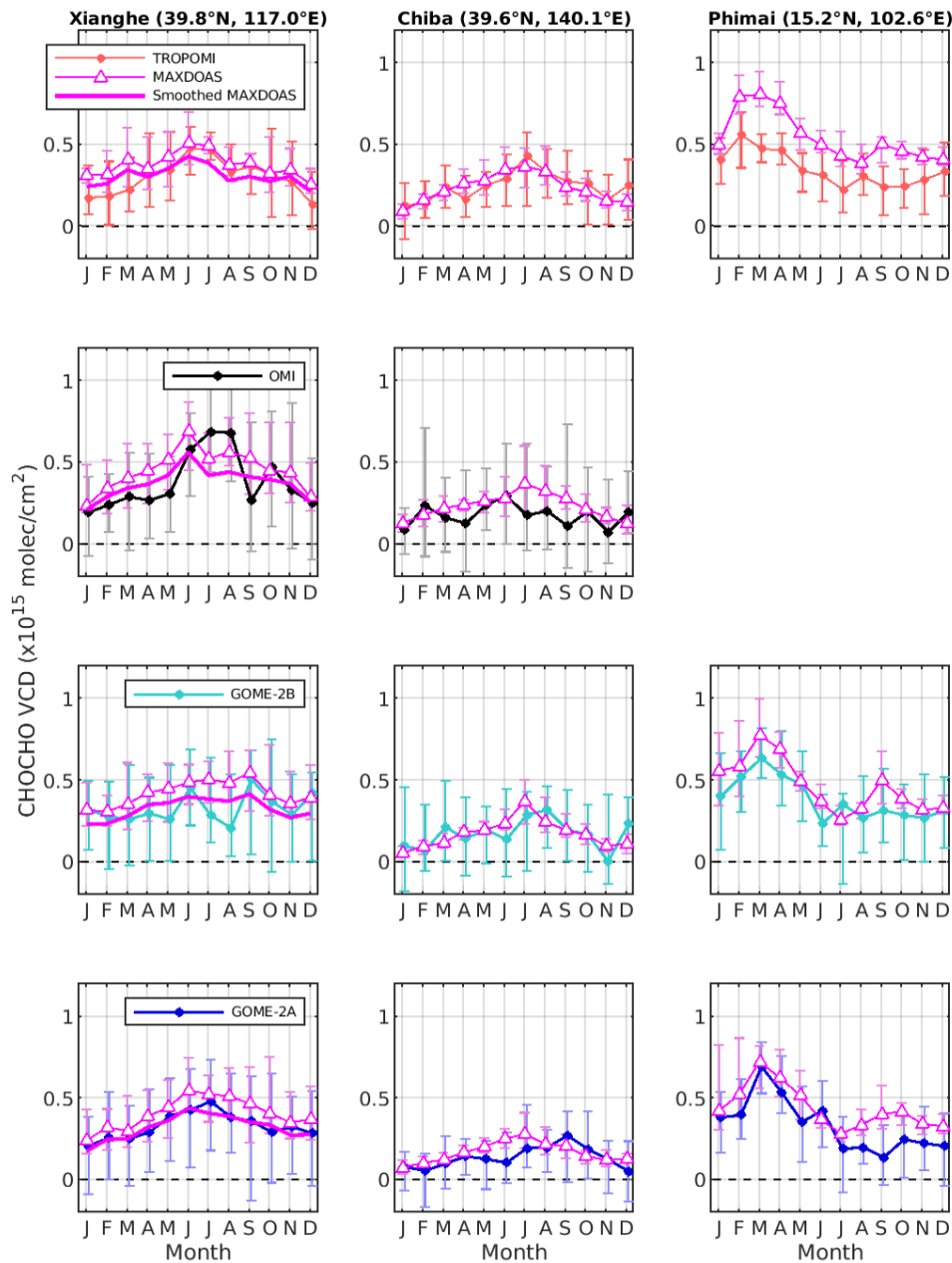


Figure 5-5: Comparison of the monthly median glyoxal tropospheric vertical column seasonal cycle as retrieved from TROPOMI, OMI, GOME-2A/B and MXD in Xianghe (China), Chiba (Japan) and Phimai (Thailand). The columns correspond to the three stations and the rows to the different satellites. In Xianghe, MXD data smoothed with the satellite averaging kernels are also shown. The error bars represent the interannual variability (25% and 75% percentiles based on the full time series available).

In Figure 5-6, we compare again the seasonal cycle of glyoxal VCDs retrieved from TROPOMI with that from more recent MAX-DOAS time series at six different stations. Four of them are located at mid-latitude in Europe and show relatively low glyoxal columns, while much larger values are measured at the two other stations, in Northern India. In Vienna and Athens, TROPOMI and MAX-DOAS glyoxal columns agree very well and show consistent seasonal dependences with maximum and minimum values during summertime and wintertime, respectively. On the other hand, at the higher latitude stations of Bremen and Uccle, the consistency of the seasonal variations seen from space and from the ground is somewhat poorer. While the glyoxal columns agree well during summertime, the satellite columns tend to underestimate MAX-DOAS values in winter, the latter showing almost no seasonal variation. Satellite glyoxal retrievals at those latitudes are challenging in winter because of the low sun elevation causing a low sensitivity to the lowermost atmospheric layers. For this reason, retrievals for solar zenith angles larger than 70° are filtered out, which explains the data gap in the seasonal cycles at those stations during the period November-January. The comparison at those two stations suggests that the loss of sensitivity is critical at even smaller solar zenith angles, at least in case of low glyoxal content. In Uccle, we have also tested the impact of smoothing the MAX-DOAS columns with the satellite averaging kernels (similarly to what was done in Xianghe), which turned out to be very small. Although the variability of the Athens data is low with exception of summer months (June-July-August), the absence of any seasonal dependence in the cities of Uccle (Brussels) and Bremen, in contrast to the Vienna and Athens, is to some extent surprising. One must however keep in mind that glyoxal retrievals from MAX-DOAS measurements are also challenging and it cannot be excluded that uncertainties in ground-based data also partly contribute to the observed differences.

In Mohali and Pantnagar, glyoxal columns are much larger and the seasonal variability is driven by fire emissions and meteorological factors such as the monsoon. At those two stations, the glyoxal seasonal variability is excellently reproduced by TROPOMI. In terms

of absolute values, the TROPOMI columns agree reasonably well in Mohali but, in Pantnagar, they significantly underestimate the (large) MAX-DOAS columns. The reason why the systematic satellite/ground-based bias is so different between those two stations is unclear. MAX-DOAS columns are clearly higher in Pantnagar than in Mohali pointing to possible local differences in air quality, not reflected in the satellite data, or to inconsistencies in the ground-based data sets. Although the agreement is excellent in Mohali, the typical behaviour is an underestimation of the columns by the satellites, as discussed before. In addition, those sites are significantly contaminated by aerosols, which are neglected in the satellite retrievals (apart from the stringent cloud filtering). MAX-DOAS data have also been analysed using very different approaches, which may also cause differences. Therefore, no real conclusion on the absolute glyoxal columns can be drawn at this stage. To address this, a more detailed analysis would be needed, which would require an homogenization of the MAX-DOAS data treatment, a more sophisticated approach for the computation of the satellite AMFs and possibly some independent information on the glyoxal vertical distribution. It is already remarkable to have such a nice consistency in the glyoxal column seasonal variability observed by the different systems.

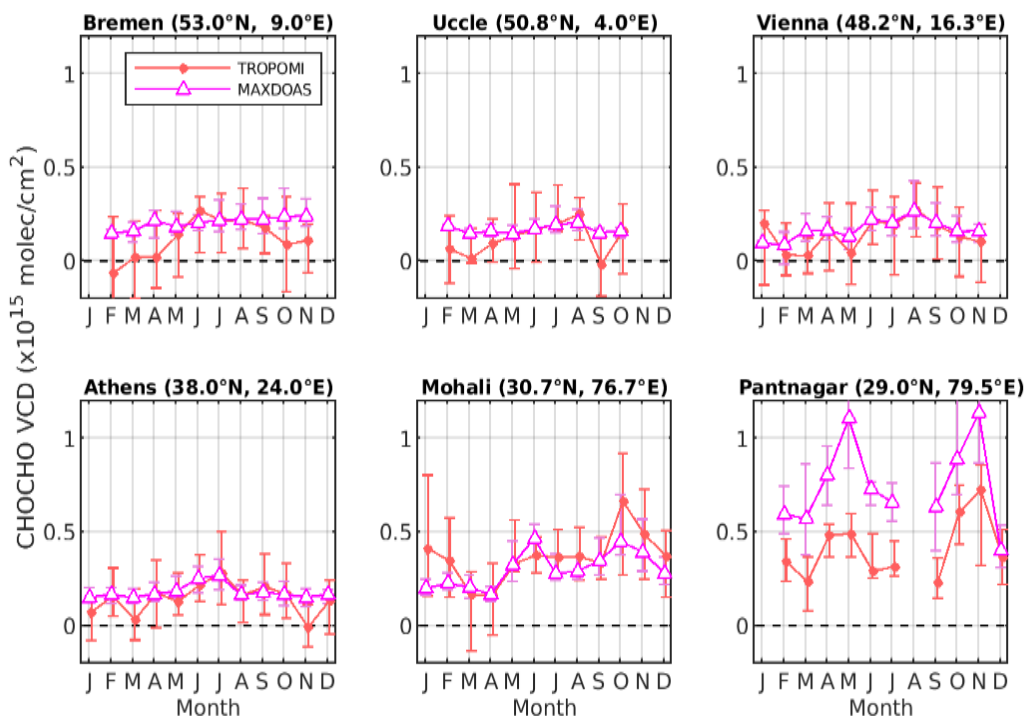


Figure 5-6: Comparison of the monthly median glyoxal tropospheric vertical column seasonal cycle as retrieved from TROPOMI and MXD at four European stations (Bremen, Uccle, Vienna, Athens) and at two Indian stations (Mohali, Pantnagar). The error bars represent the interannual variability (25% and 75% percentiles based on the full time series available).

5.1.3. Dependence on influence quantities

It has been found that the validation results were poorer over European regions at high latitudes where the glyoxal signal is weaker and the sun elevation lower, making the retrieval conditions more challenging. Also the impact of factors such as clouds and aerosols are also at the origin of a larger scatter in the observed differences between CHOCHO columns from MAX-DOAS and those columns from GLYRETRO.

5.1.4. Bias and short term variability

Table 5-2 also gives the mean bias as derived from the comparison of the satellite and MAX-DOAS glyoxal column seasonal cycle as well as the standard deviation of the differences. As discussed above, the mean differences are generally less than 1×10^{14} molec/cm², except for high column conditions where differences are noticeably higher.

Table 5-2: Correlation coefficients between the satellite and MAX-DOAS monthly median glyoxal tropospheric vertical columns as well as mean absolute difference and associated standard deviation at nine stations. Only a few MAX-DOAS stations offer a time series long enough (see Table 4-1) to make the analysis possible for the OMI and GOME-2A/B instruments.

	TROPOMI	OMI(until 2013)	GOME-2B (until 2016)	GOME-2A
	Correlation coefficient			
	Mean bias \pm standard deviation ($\times 10^{14}$ molec/cm ²)			
Xianghe	0.87 -0.8 \pm 0.6	0.70 -0.7 \pm 1.3	0.37 -0.9 \pm 0.9	0.92 -0.8 \pm 0.4
Chiba	0.80 0.1 \pm 0.6	0.32 -0.6 \pm 0.8	0.66 0.0 \pm 0.7	0.58 -0.1 \pm 0.9
Phimai	0.85 -2.0 \pm 0.8	N/A	0.88 -0.8 \pm 0.8	0.86-1.1 \pm 0.8
Bremen	0.13 -0.9 \pm 0.9	N/A	N/A	N/A
Uccle	0.67 -0.5 \pm 0.7	N/A	N/A	N/A
Vienna	0.73 -0.3 \pm 0.6	N/A	N/A	N/A
Athens	0.61 -0.4 \pm 0.6	N/A	N/A	N/A
Mohali	0.70 0.6 \pm 0.9	N/A	N/A	N/A
Pantnagar	0.78 -3.5 \pm 1.5	N/A	N/A	N/A

Overall, the figures presented before show that the short-term variability seen in the MAX-DOAS measurements is nicely reproduced by GLYRETRO. Table 5-2 provides an overview of the correlation coefficients between the satellite and the MAX-DOAS glyoxal columns at all considered stations. For stations where the analysis was possible for all satellite sensors, the correlation coefficients are significantly better for TROPOMI than

for other instruments. It is also clear that correlation coefficients are better for sites characterised by large and highly variable glyoxal columns (e.g. Asian vs European stations). Apart from the Bremen station where the negative bias during winter leads to a low correlation coefficient, all other values are quite reasonable and range between 0.61 and 0.87 for TROPOMI.

5.1.5. Status of validation

So far the validation of the S5P TROPOMI glyoxal vertical column data is mainly based on satellite to MAX-DOAS comparisons, for which good agreement is found, but also complemented with comparisons with other satellite and model data (see after). Validation for regions using ground based MAX-DOAS data is limited to Europe and Asia regions (Xianghe, Beijing, Pantnaga, Phimai, Athens, Bremen, Vienna, Chiba, Kasagua). In addition, MAX-DOAS data is not retrieved in a homogenous way, which would be beneficial in the future for improving the validation of glyoxal satellite data.

5.2. Inter-satellite comparison.

5.1.6. TROPOMI inter-algorithm comparison

In this section, GLYoxal Retrievals from TROPOMI are compared with columns retrieved using the IUP-UB Glyoxal retrieval for TROPOMI (Table 5-3). The IUP-UB glyoxal retrieval is based on settings described in Alvarado et al. (2020). This comparison enables to identify possible differences introduced by specific algorithm features such as fit window, CTM model, background correction, etc.

Figure 5-7 compares the multi annual average of glyoxal maps for the two algorithms for the period from 2018 to 2020. Significant differences are observed between both retrievals with a clear low bias for IUP-UB. Although the two algorithms are similar in many aspects, there also exist differences such as the a priori model profiles, and the background correction.

Table 5-3: GLYRETRO and IUP-UB parameters used to retrieve glyoxal from TROPOMI.

Parameters	GLYRETRO	IUP-UB
Fitting window	435-460 nm	433-465 nm
Polynomial	4 coefficients	5 coefficients
Cross-sections used:		
CHO.CHO (Volkamer et al., 2005)	Yes (296 K)	Yes (296 K)
NO2 (Vandaele et al., 1998)	Yes (220K, 2294 K)	Yes (220K, 2294 K)
O4 (Thalman et al., 2013)	Yes (293 K)	Yes (293 K)
O3 (Serduchenko et al., 2014)	Yes (223 K)	Yes (223 K)
H2O (Rothman et al., 2013)	Yes (296 K)	Yes (296 K)
Liquid water (Mason et al., 2016)	Yes (280 K)	Yes (280 K)
Ring effect	Ring cross section	
Heterogeneity pseudo-cross-sections	Yes	No
Iterative spike removal (Richter et al., 2011)	Yes	Yes
Intensity offset correction	Linear offset (I/I ₀)	
Background spectrum	Pacific region (one per row and per day)	
Model profiles	MAGRITTE CTM	TM5PM
Profiles over ocean region	Single profile from TORERO campaign	Model profiles (TM5)

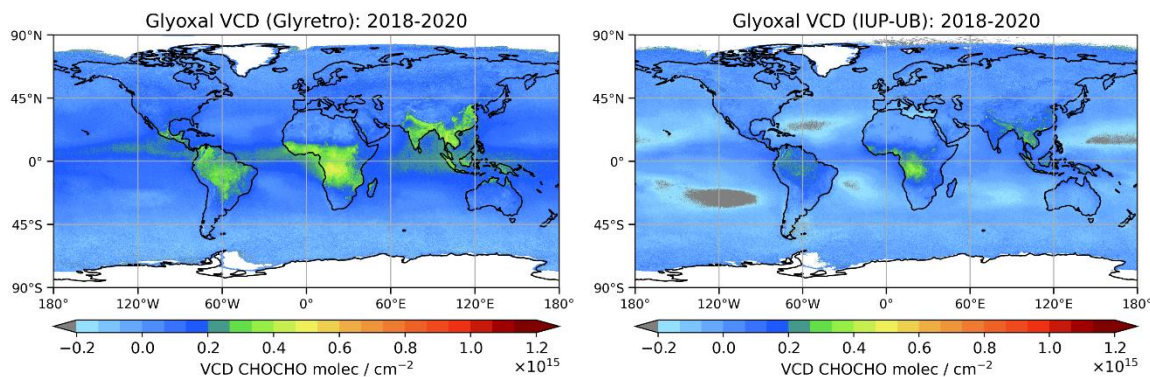


Figure 5-7 Comparison of multi annual averages of glyoxal columns as derived with GLYRETRO (left) and IUP-UB (right) retrievals from TROPOMI observations from 2018 to 2020.

Similar to VCD multi annual averages, glyoxal SCD also show large differences between products (see Figure 5-8). This can be understood by the different offset corrections applied in both products. While IUP-UB uses a mean model value computed over the reference region, GLYRETRO introduces a constant value of $1 \times 10^{14} \text{ molec cm}^{-2}$. In order

to evaluate the impact of the background correction, the IUP-UB retrieval was modified by replacing the model mean value with a constant value as in GLYRETRO. Figure 5-9 shows the multi annual average of the background-corrected SCD for GLYRETRO and the modified IUP-UB retrievals. As can be seen, the agreement is much improved, indicating the importance of the offset correction in the glyoxal retrievals.

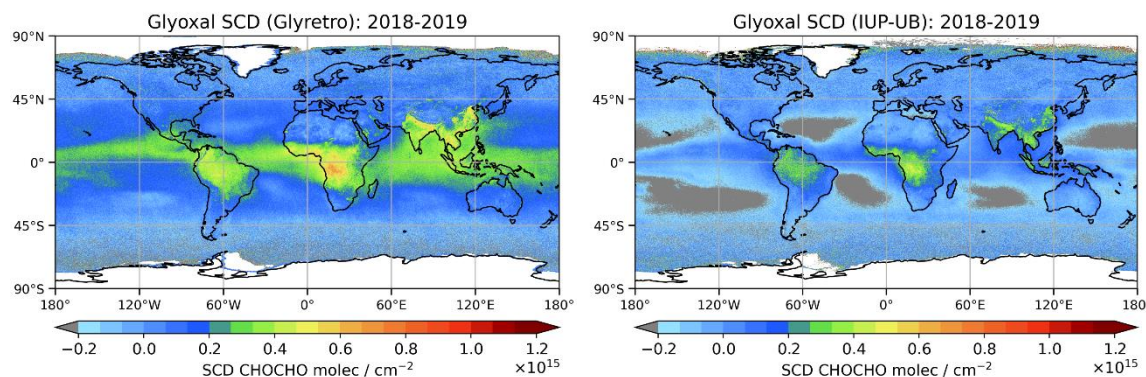


Figure 5-8: Comparison of glyoxal raw SCD multi annual average as derived with GLYRETRO (left) and IUP-UB (right) retrievals from TROPOMI observations from 2018 to 2019.

For a closer comparison, time series have been computed for both products for six different regions including North America, South America, Europe, Africa north of the equator, Africa south of the equator, and China. Figure 5-10 shows time series of glyoxal SCD for the selected regions (see Table 5-4).

Table 5-4: Regions selected for figures Figure 5-10, Figure 5-12 and Figure 5-14.

Region	Latitude[°]	Longitude[°]
North America	34±6	84±10
South America	-9±7	60±12
Europe	45.5±9.5	8±20
Africa north of equator	6±5	10.5±25.5
Africa south of equator	-8±7	22.5±9.5
China	30±10	116.5±6.5

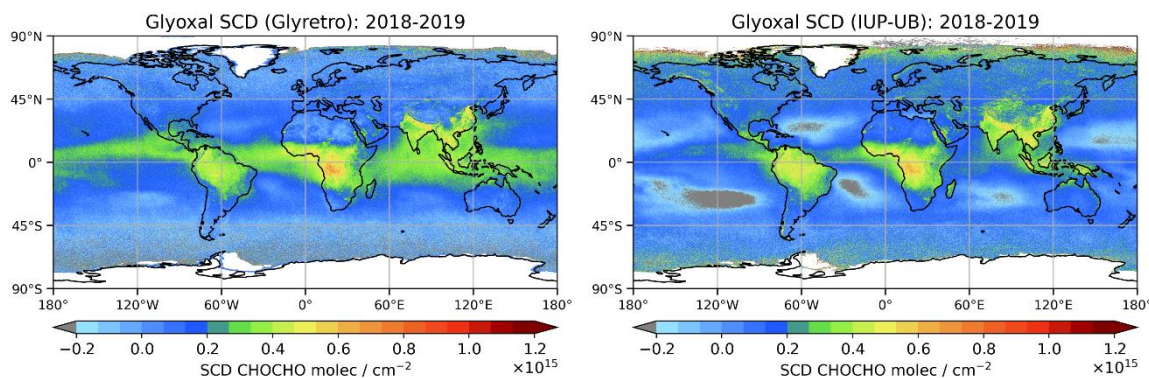


Figure 5-9: Comparison of glyoxal normalized SCD multi annual average as derived with GLYRETRO (left) and IUP-UB (right) retrievals by using a consistent reference value of 1×10^{14} molec.cm⁻².

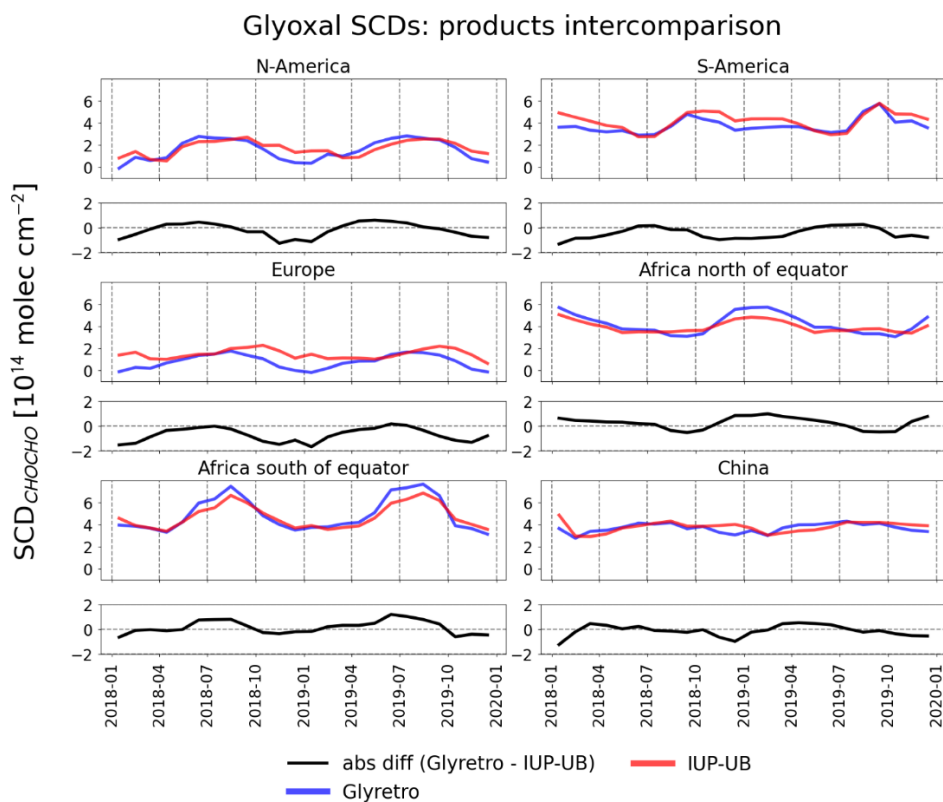


Figure 5-10: Comparison of monthly averaged glyoxal SCDs from GLYRETRO (blue line) and IUP-UB (red line) retrievals for 6 selected regions over different environments during 2018-2019. At the bottom of each subplot, absolute differences are shown for each region (black line) for the same period.

The replacement of model mean value by a constant value as in GLYRETRO led to similar SCD amounts in both retrievals, showing the impact of offset correction in the absolute glyoxal levels. However, still some differences are observed between products, especially over ocean and to a lesser degree in some continental regions.

Another important driver of possible differences between the two products is the AMF, which is computed based on two different model output, while GLYRETRO uses the CTM MAGRITTE; which inherits from the IMAGES model (Bauwens et al., 2016, Müller and Brasseur, 1995; Stavrakou et al., 2013), IUP-UB uses TM5PM (Myriokefalitakis et al., 2020). Figure 5-11 shows multi annual averages of the AMF used in GLYRETRO and IUP-UB retrievals. The global pattern is similar between both products, but IUP-UB AMFs are lower than those for GLYRETRO. In order to investigate the temporal evolution, time series of monthly mean AMFs are compared for the six selected regions in Figure 5-12.

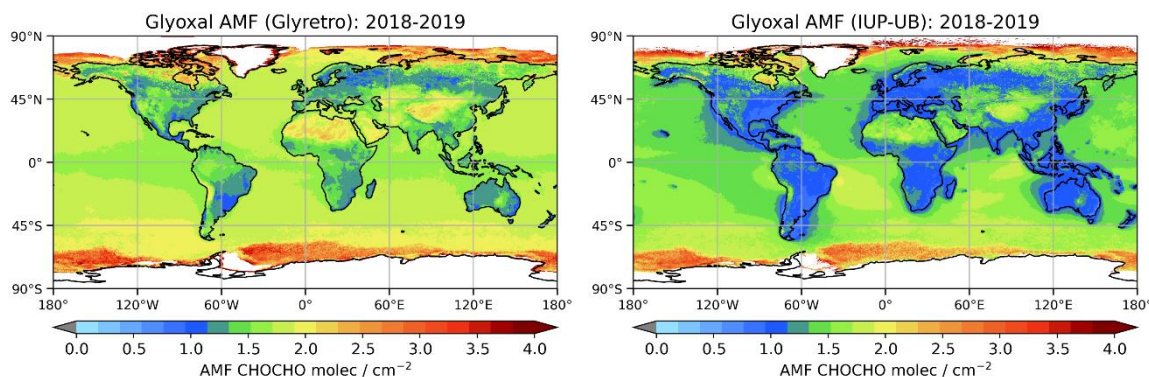


Figure 5-11 Comparison of glyoxal AMF multi annual average used in the conversion of SCD to VCD for GLYRETRO (left) and IUP-UB (right) for TROPOMI measurements from 2018 to 2019.

Significant differences are found between products for the different regions, with generally larger values for GLYRETRO than for IUP-UB. However, these differences are compensated by the offset correction and bias between products are reduced. Thus, from

now on comparison will be focused on the products using a background correction with a constant value.

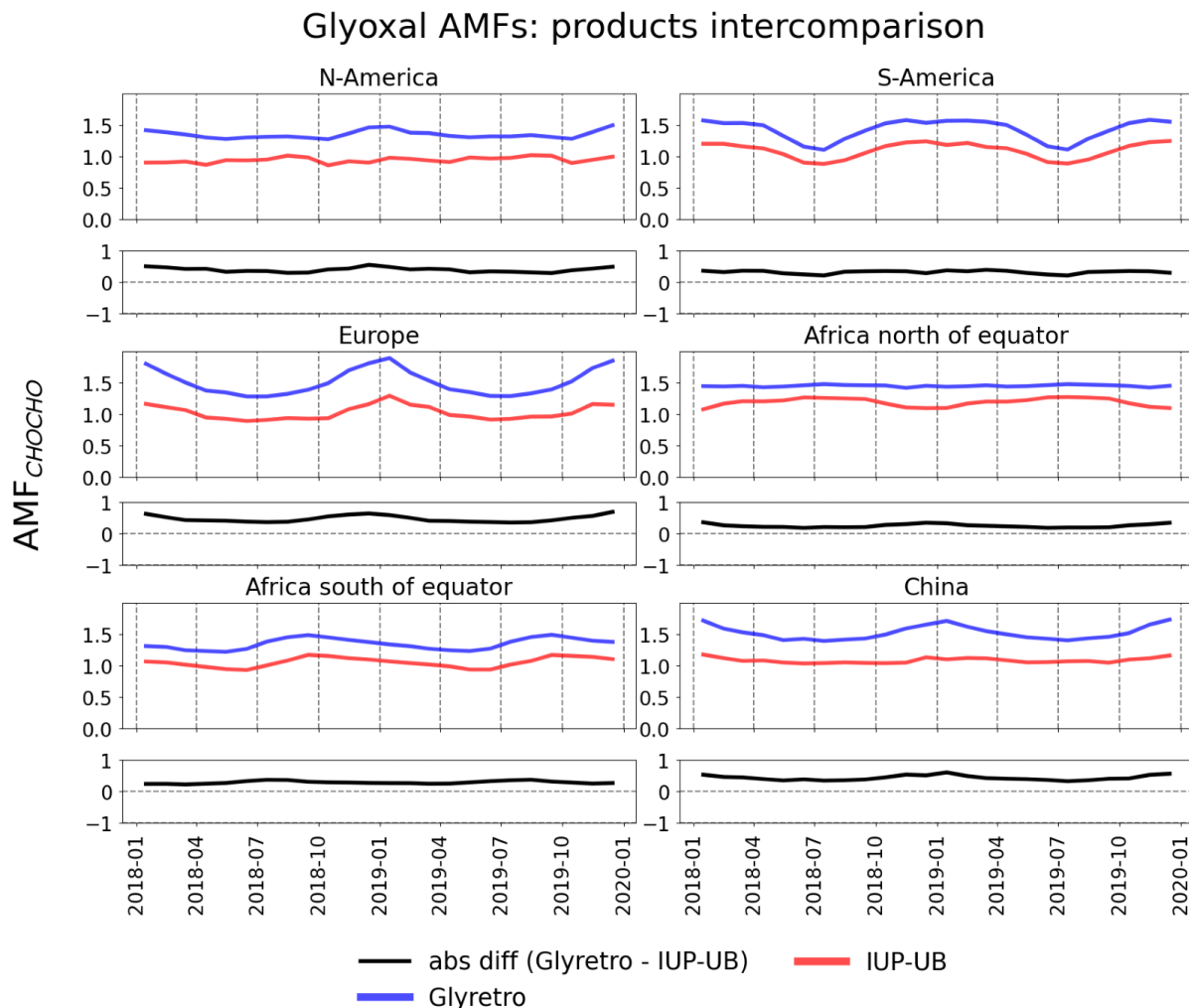
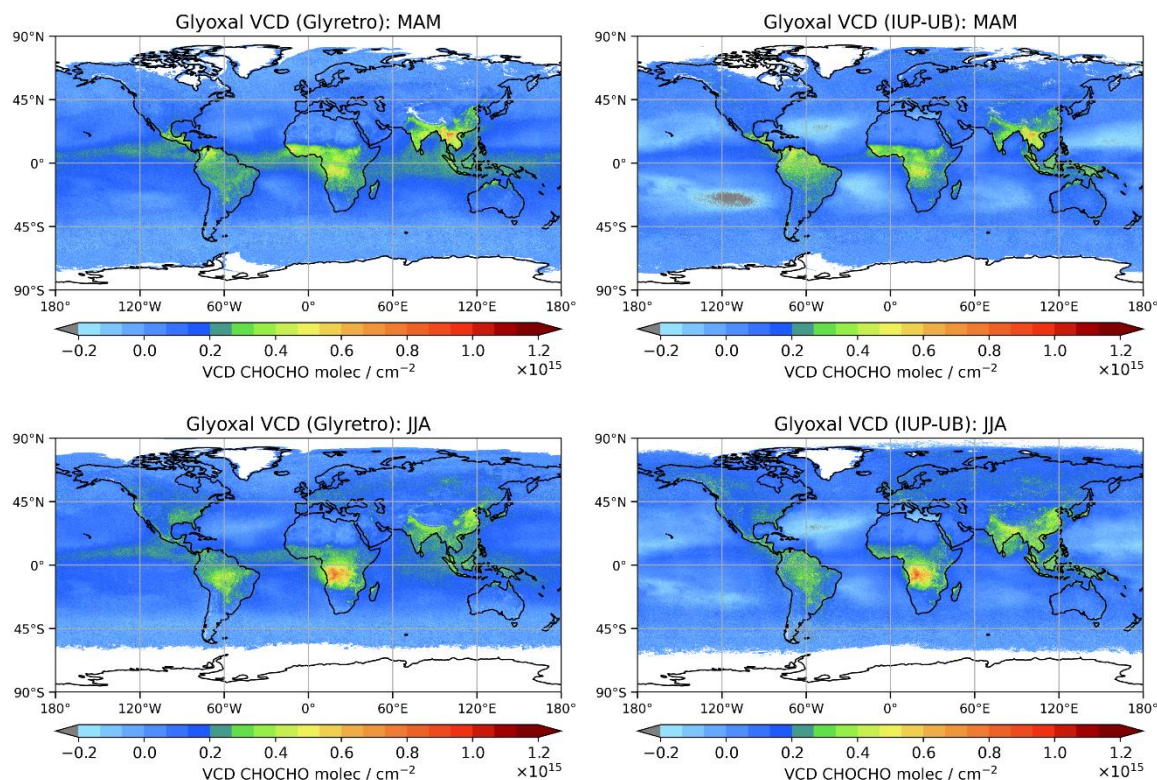


Figure 5-12: Comparison of monthly averaged glyoxal AMFs from GLYRETRO (blue line) and IUP-UB (red line) retrievals for 6 selected regions over different environments during 2018-2019. At the bottom of each subplot, absolute differences are shown for each region (black line) for same period.

Figure 5-13 compares seasonal glyoxal maps for both products, when considering observational averaged over 3 years period. These maps for GLYRETRO and IUP-UB show very similar patterns both in terms of the geographic distribution of the glyoxal

signal and of their magnitude. There are some differences over oceanic region most likely introduced by the different approach used for account the glyoxal signal in this region (e.g. GLYRETRO uses a single profile from TORERO campaign). Also, DOAS parameters play an important role in the observed columns over oceans (e.g. fit window) as will be discussed at the end of the section. There is no clear systematic bias between the products, however some differences are observed for some seasons. The largest glyoxal VCDs are found during the warm season and over Tropical regions, while at high latitudes glyoxal columns are low and depend on biogenic activities during summer.



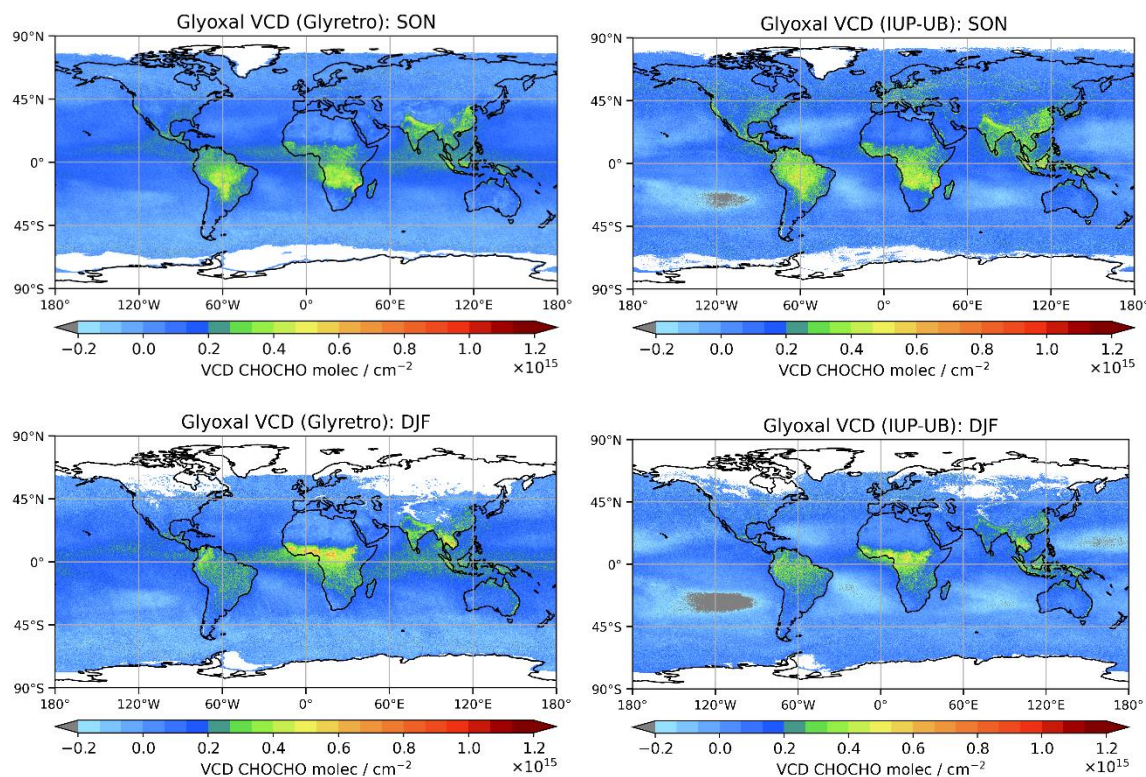


Figure 5-13: Comparison of glyoxal VCD seasonal maps (MAM: March-April-May, JJA: June-July-August, SON: September-October-November, DJF: December-January-February) as derived from GLYRETRO (left) and IUP-UB (right) for TROPOMI observations.

Figure 5-14 shows time series of glyoxal VCDs for GLYRETRO and IUP-UB products as well as glyoxal from the TM5 model for six regions over continental areas. The maxima observed for the three products correspond to the warm season and are found in the same period. The background signal for TM5 is slightly lower than those from GLYRETRO and IUP-UB. Also, regions with expected large anthropogenic emissions such as Europe and China do not show variability for TM5 which is in contrast to the behaviour observed by GLYRETRO and IUP-UB products. As already pointed out, GLYRETRO and IUP-UB products show a very similar temporal evolution with differences only in specific months, most likely introduced by the different a priori profiles used in the two products.

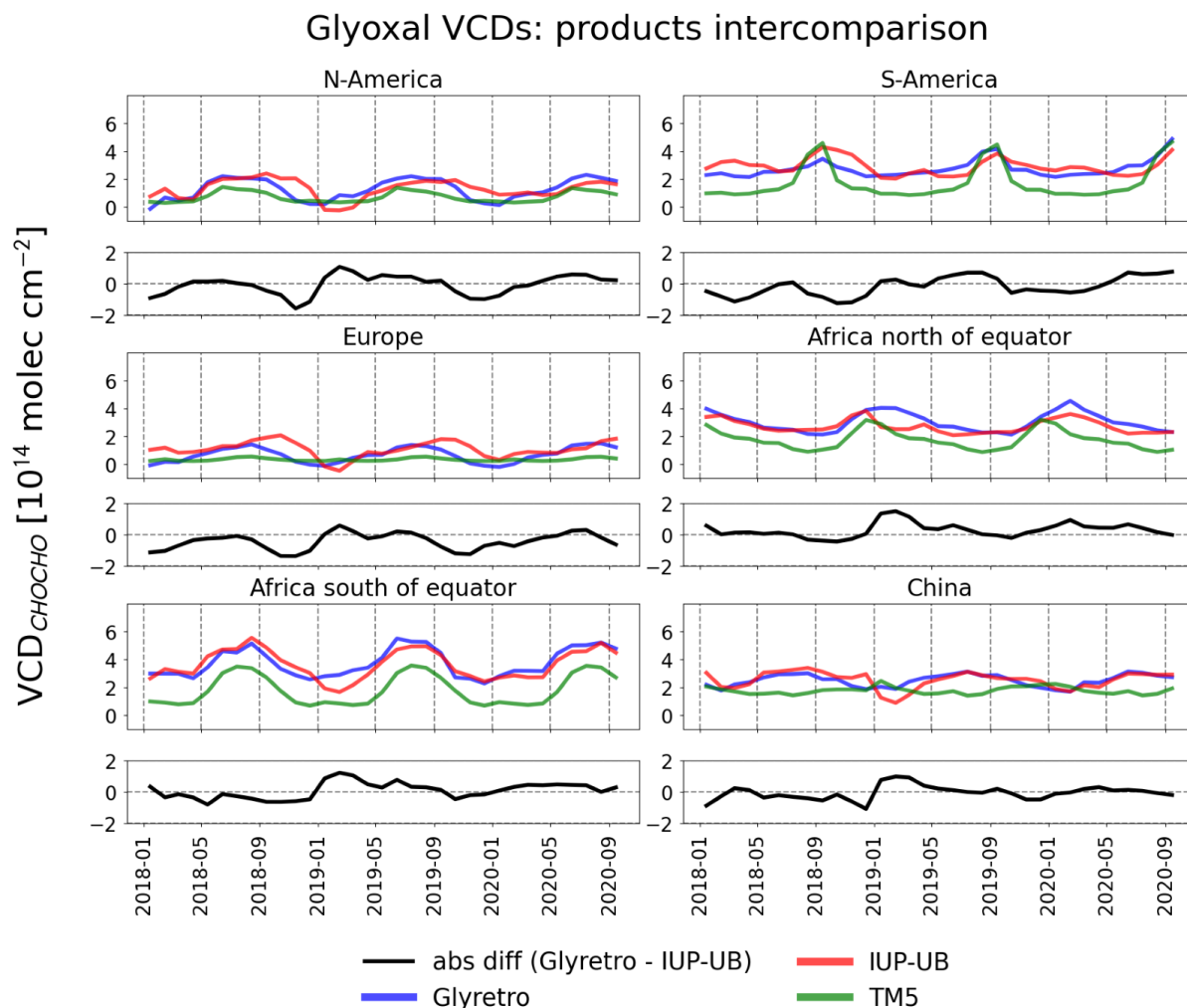


Figure 5-14: Comparison of monthly averaged glyoxal VCDs from GLYRETRO (blue line), IUP-UB (red line), and TM5 (green line) products for 6 selected regions over different environments during 2018-2020. At the bottom of each subplot, absolute differences are shown for each region (black line) for the same period between GLYRETRO and IUP-UB.

Although the differences between products are generally small, some of them are unclear and are probably introduced by the different DOAS parameters used in the fit. One of the key parameter is the fit window, as it influences the cross correlation effects between the different absorbers (Alvarado et al., 2014). Here, an example test is presented in order to evaluate only the effect of fit window in the glyoxal retrieval. Figure 5-15 shows

comparison of multi annual averages of VCDs from 2018 to 2020 for GLYRETRO, IUP-UB and an additional retrieval, which is identical to the IUP-UB product but uses a different fit window (433-463 nm). The maps show similar glyoxal distributions; however, the retrieval using the fit window between 433 and 463 nm has larger columns over oceanic regions, similar to GLYRETRO but lower values over continental regions than the other two products.

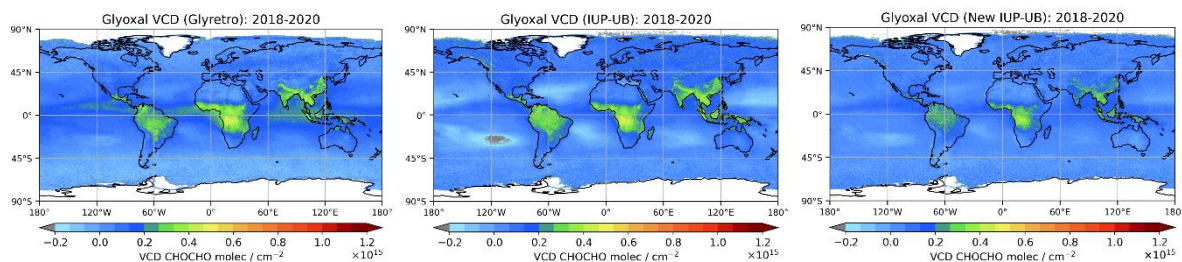


Figure 5-15: Comparison of glyoxal column multi annual average as derived with GLYRETRO (fit window: 435-460 nm, left), IUP-UB (fit window: 433-465 nm, centre), and New-IUP-UB (fit window: 434-463 nm, right) retrievals from TROPOMI observations from 2018 to 2020.

5.1.7. Inter-sensor comparison

In this section, TROPOMI glyoxal tropospheric columns are compared with columns from OMI and GOME-2A/B, generated with the same retrieval algorithm developed by BIRA-IASB. For GOME-2A and B, we use data records recently produced within the operational environment of the EUMETSAT AC SAF (Valks et al., 2020), based on retrieval settings recommended following our algorithmic baseline. This comparison allows identifying possible differences due to instrumental features.

Figure 5-16 and Figure 5-17 compare seasonal glyoxal field maps from the four satellite instruments, when considering observations averaged over long periods. Those maps show very similar patterns both in terms of the geographic distribution of the glyoxal signal and of its amplitude. There is no clear systematic bias between the different

products. The largest glyoxal columns are generally observed in Tropical regions. At mid-latitudes, glyoxal columns are generally lower but increase during summertime as a response to biogenic activity.

Glyoxal columns increase significantly during fire events. Regions with large scale fires such as Amazonia, Africa, India, Thailand have the largest glyoxal columns. The intensity of those fires may change from a year to another, which causes a significant inter-annual variability. For example, Figure 5-18 shows OMI and TROPOMI time series of glyoxal over Amazonia where intense fires take place generally in the period August-October and a maximum in the glyoxal columns is seen at this period. However, there is a large interannual variability in the number of fires and their intensity, which directly impacts the amplitude of the glyoxal peaks. The right panel of the Figure 5-18 shows a time series of estimates of fire emissions in this region and there is a 1-to-1 correspondence between years with large emissions and large observed glyoxal columns. We also see on this figure that TROPOMI nicely extends the OMI time series. Another example of this is in Souteastern Australia where TROPOMI has observed very large glyoxal columns due to the intense fires that took place in January 2020. Due to the limited number of years in the TROPOMI time series, we see in that region larger glyoxal columns in the TROPOMI map for December-January-February (Figure 5-17) compared to the other sensors.

Anthropogenic emissions in highly populated area may also lead to elevated glyoxal columns. Hot spots of glyoxal over megacities like Beijing, Bangkok, Johannesburg, Mexico, New Delhi, Teheran, Sao Paulo are detected in the OMI and TROPOMI maps. Those hot spots are generally no so well resolved in the GOME-2 maps because of both the coarser spatial resolution of the observations and the limited amount of data.

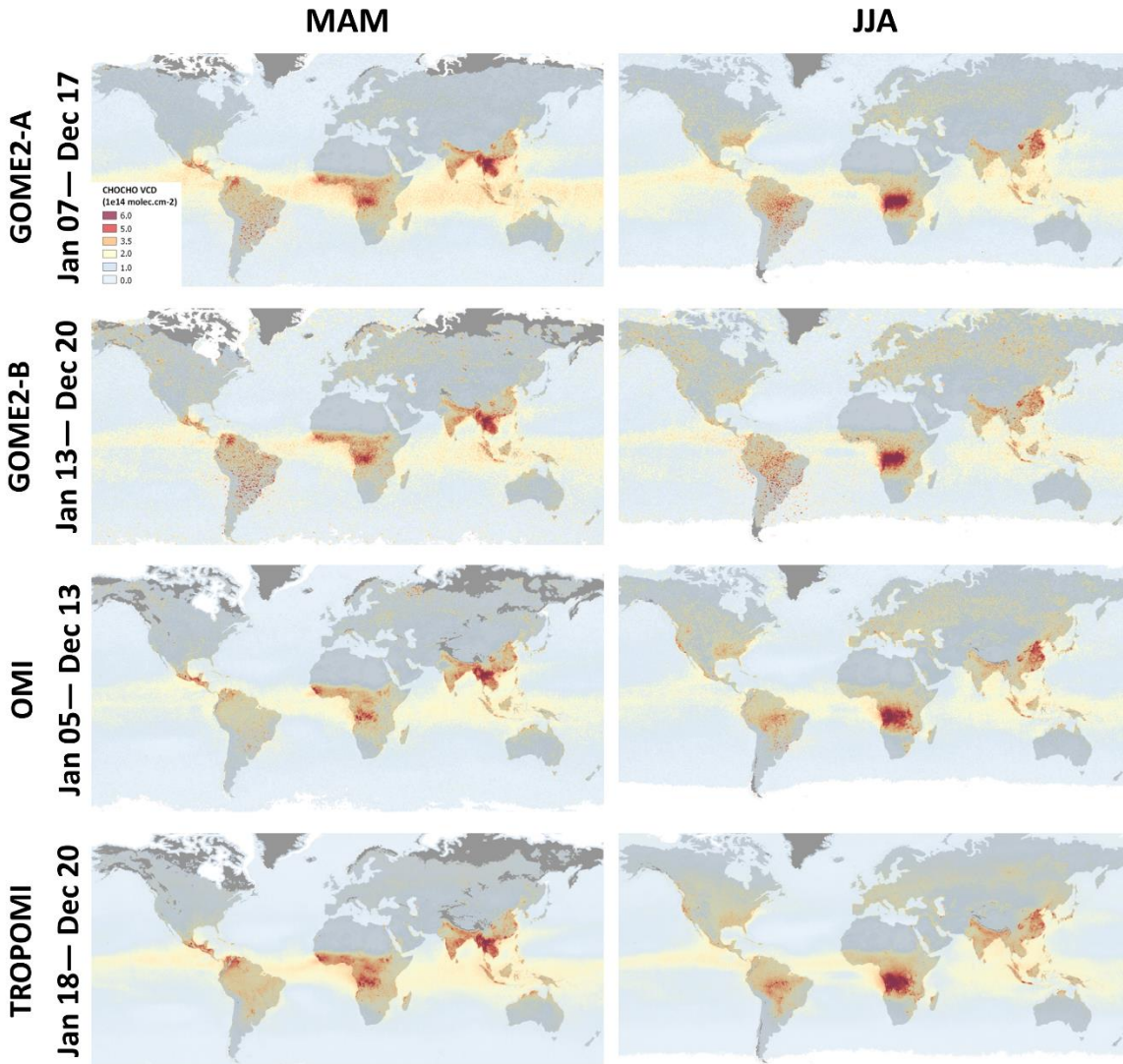


Figure 5-16: Comparison of glyoxal column ($\times 10^{14}$ molec.cm⁻²) seasonal maps (March/April/May and June/July/August) as derived from OMI, GOME-2A, GOME-2B and TROPOMI observations. Those maps have been produced by combining observations over long periods (G2A: 2007-2017; G2B: 2013-2020; OMI: 2005-2013; TROPOMI: 2018-2020).

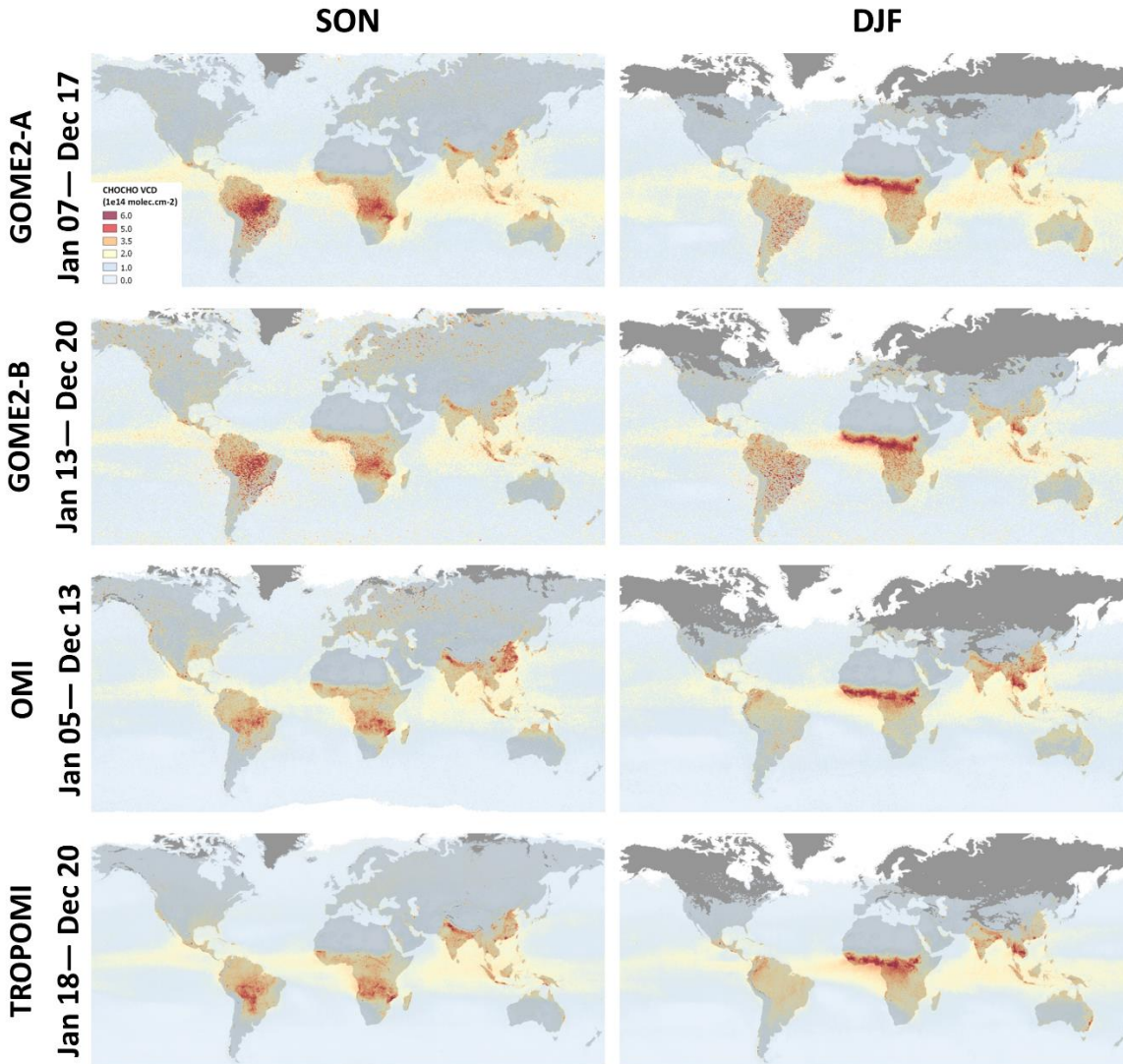


Figure 5-17: Comparison of glyoxal column ($\times 1e14 \text{ molec.cm}^{-2}$) seasonal maps (September/October/November and December/January/February) as derived from OMI, GOME-2A, GOME-2B and TROPOMI observations. Those maps have been produced by combining observations over long periods (G2A: 2007-2017; G2B: 2013-2020; OMI: 2005-2013; TROPOMI: 2018-2020).

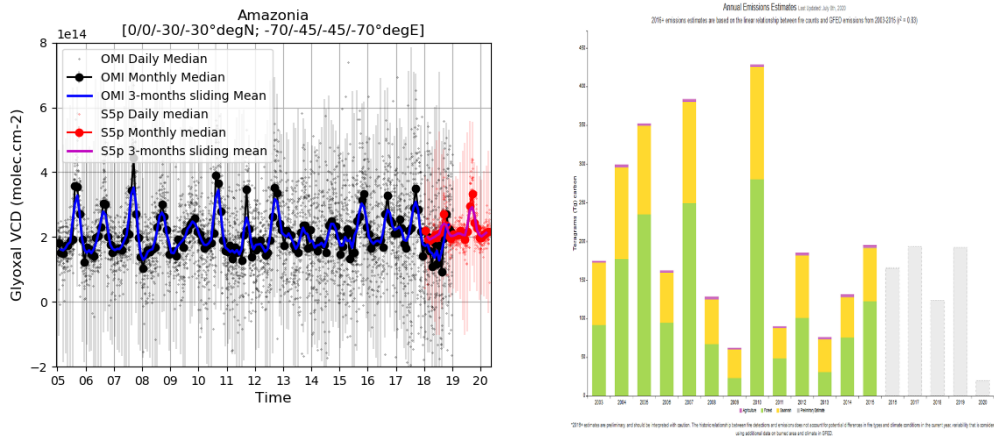


Figure 5-18: Left panel: Time series of glyoxal columns in Amazonia as seen by OMI and TROPOMI. As indicated in the legend, different curves show daily, monthly and 3-months smoothed median values. Right panel: Annual emissions estimated from the Global Fire Emissions Database in Amazonia. (Figure taken from <https://www.globalfiredata.org>).

Figure 5-19 compares the full glyoxal time series from the four instruments in different regions worldwide covering different types of emissions and Figure 5-20 shows the corresponding typical seasonal cycles when combining all years together. All those different time series show an overall good consistency in terms of amplitude and seasonal variations. In Tropical regions, the four data sets are relatively stable and show similar seasonal cycles and column values, although OMI appears to be slightly lower than the others, in particular in Equatorial Africa. In Asia, the many glyoxal hot spots are caused by different types of emissions. In addition to biogenic activities, large emissions due to fires may significantly contribute to the glyoxal columns. For example, in Northern India, two fire seasons in April/May and October/November lead to two glyoxal maxima per year. In addition, strong anthropogenic emissions occur in this highly populated region like in North-eastern China, where glyoxal column remain elevated during wintertime, while biogenic emissions are low. At mid-latitudes, the retrievals are more challenging because of the lower sun elevation. Nevertheless, the small seasonal cycles from the 4 satellites agree. Nevertheless, during wintertime, TROPOMI columns appear slightly lower than those from the other satellites. In addition, the stability of the OMI record at mid-latitudes is degraded after 2014, which likely originates from the evolving row

anomaly leading to an increased number of outliers. In the Indo-Gangetic Plains, OMI columns often deviate from the other sensors for the same reason.

Figure 5-20 also shows the seasonal cycle as modelled by the CTM MAGRITTE using emission inventories of 2018, which is generally in good agreement with the observations. Although there are obviously some larger differences in the absolute column numbers, the seasonal variations are very consistent, even in strongly polluted regions like China. On the other hand, in the Indo-Gangetic Plains, the double annual maxima is not well captured by the model, which would deserve further investigation. This overall good agreement with the model gives nevertheless confidence into the physical soundness of the measurements.

A statistical analysis based on a larger number of regions than those discussed here shows that the inter-satellite differences are, on average, less than 5×10^{13} molec/cm² (20%). This analysis confirms that applying a common retrieval baseline to different satellite instruments leads to consistent data sets, which might be combined together in longer time series.

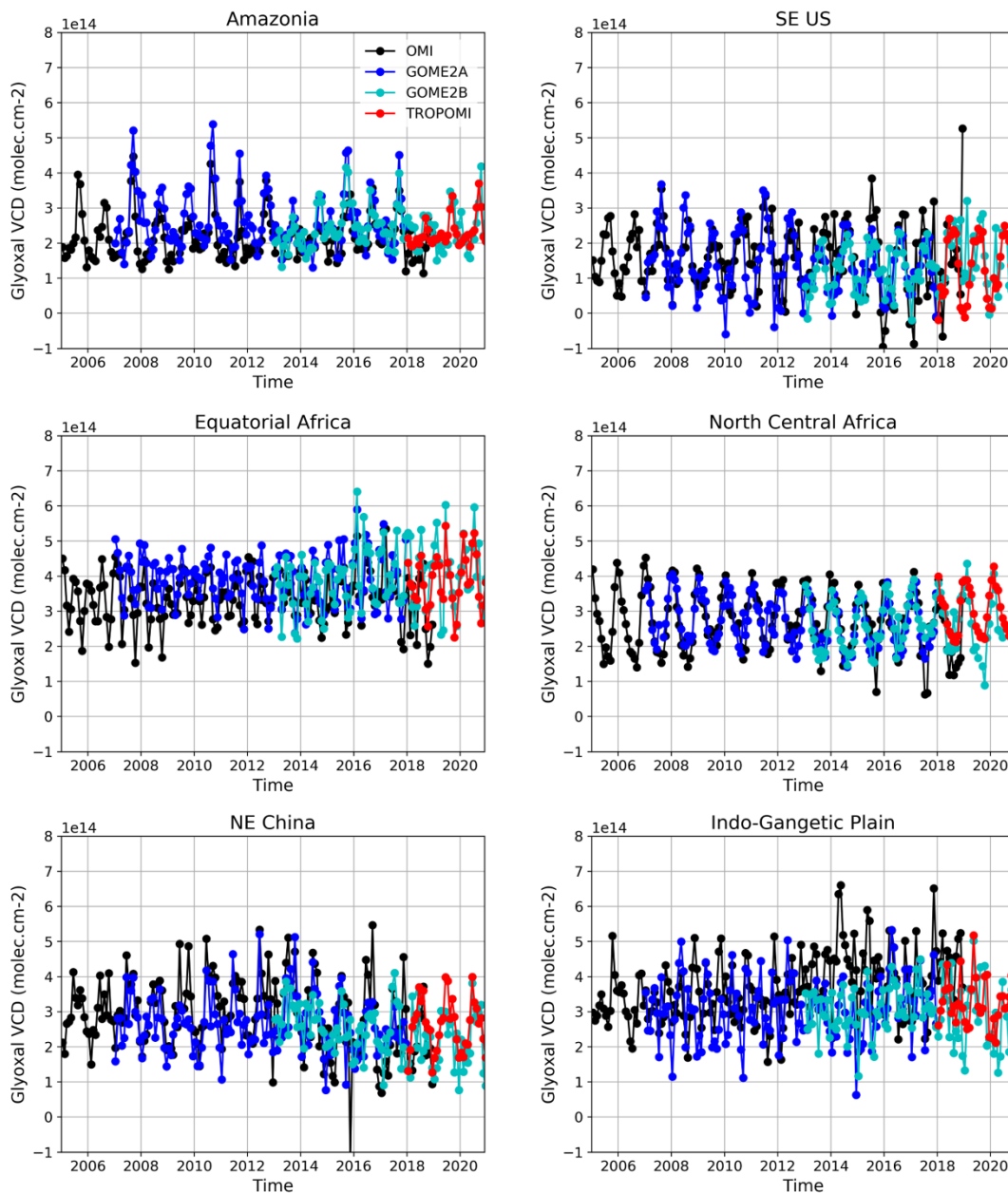


Figure 5-19: Time series of monthly mean glyoxal columns as seen by OMI, GOME-2A, GOME-2B and TROPOMI in different regions worldwide.

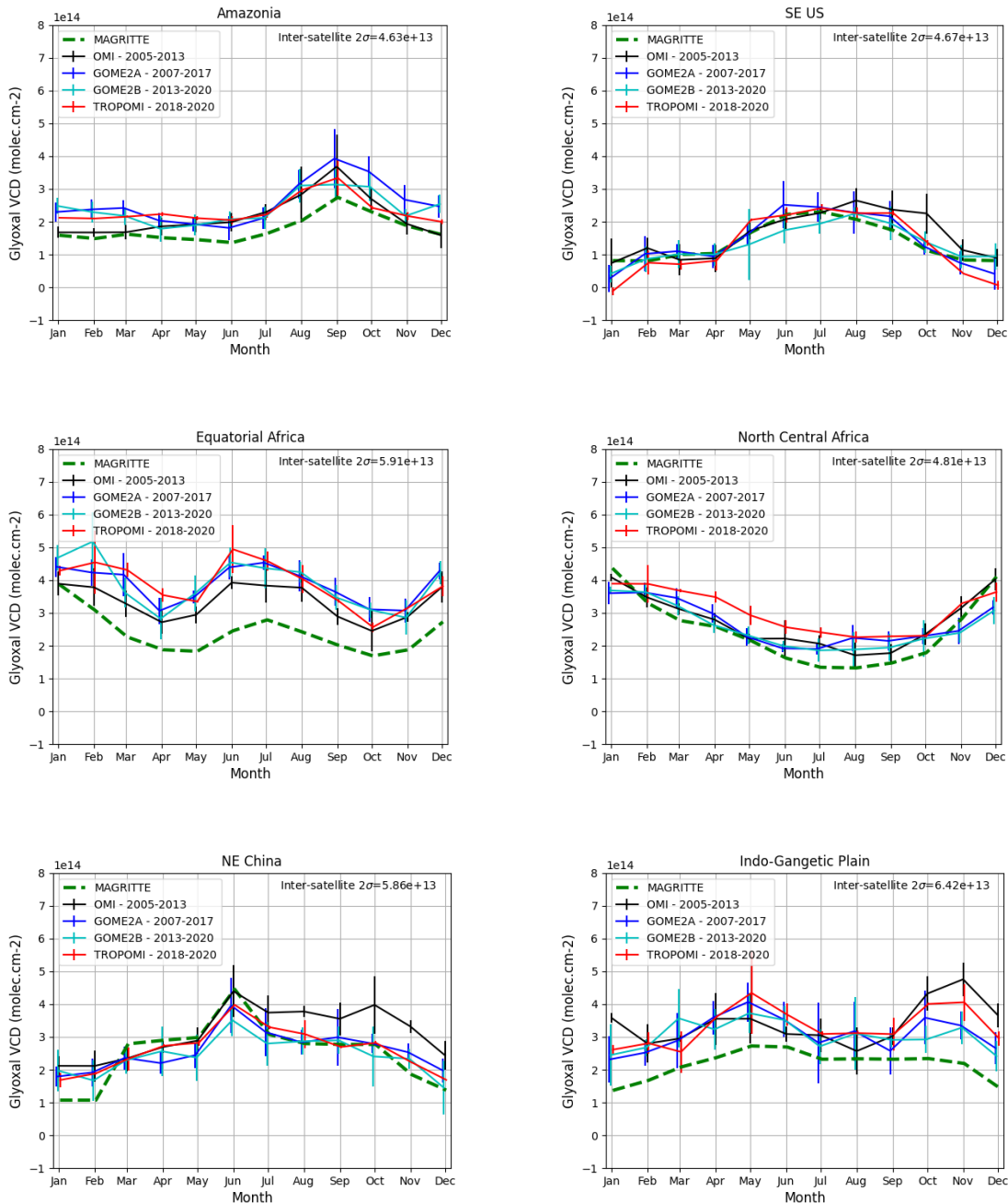


Figure 5-20: Comparison of the seasonal cycles observed from OMI, GOME-2A/B and TROPOMI using the periods mentioned in the legends. The error bars represent the inter-annual variability. The seasonal cycle of the glyoxal columns modelled with the CTM MAGRITTE using emission inventories from 2018 is also drawn (dashed green curve).

6. Conclusions

Satellite observations have been compared with independent MAX-DOAS data sets from stations located in Asia and Europe. Owing to the scarcity of MAX-DOAS glyoxal data sets, especially covering several seasons, this validation exercise is therefore unprecedented. Based on a thorough analysis at the Xianghe station (China), where a 10-year time series of MAX-DOAS data is available, and on the comparison of seasonal cycles at other stations, we conclude that satellite and MAX-DOAS instruments observe consistent glyoxal signals and have similar intra-annual variations. This is reflected by the strong correlation coefficients, ranging between 0.61 and 0.87 for TROPOMI, with the exception of one mid-latitude station where the correlation is poorer. In general, the satellite and MAX-DOAS columns also agree in absolute values with differences less than 1×10^{14} molec/cm², at least for stations with moderate columns. In Xianghe, we showed that the application of the satellite averaging kernels to the MAX-DOAS data further reduces the mean differences. There are however two stations (Phimai/Thailand and Pantnagar/India) where the satellite/MAX-DOAS bias is more significant, despite a reasonable agreement of the measured seasonal variations. Although the origin of this bias is not fully understood, the MAX-DOAS columns at those stations are very high and it is not uncommon to have such biases in UV-Visible satellite retrievals for strongly polluted sites. It cannot be excluded that part of the bias originates from the MAX-DOAS retrieval strategy at those sites. We have also indications that the satellite observations are low-biased during wintertime at mid-high latitudes where both the glyoxal signal is weak and the sensitivity to the boundary layer is reduced. The comparisons of OMI, GOME-2 and MAX-DOAS glyoxal columns also show reasonable agreement and similar intra-annual variability. Both the correlation coefficients and the scatter of the satellite/ground differences were however less good than those of TROPOMI. This points again to the better performance of TROPOMI for the detection of glyoxal from space and to its enhanced capability at providing information on VOC emissions.

An intercomparison of two different TROPOMI products (GLYRETRO and IUP-UB) showed a good consistency in terms of seasonal variability and amplitudes. However, it has been identified that the offset correction is one of the main causes for possible biases between products. Another important driver for possible differences between the two products is the AMF, which is computed based on two different model outputs. Although the differences between products are generally small, some of them remain unclear and are probably introduced by the different DOAS parameters used in the fit (e.g. fit window). Indeed, the latter significantly influences the cross correlation between different absorbers, which may also introduce some systematic biases.

Inter-satellite comparisons based on TROPOMI, OMI, GOME-2A and GOME2B products generated with a common algorithm show very consistent glyoxal retrievals in terms of amplitude and seasonal variations. Differences are typically less than 5×10^{13} molec/cm² (~20%). This excellent consistency would allow in principle to combine those individual data sets to generate longer time series. It has to be noted that some instabilities appear in the OMI data record after 2013, likely due to the evolving row anomaly.

On the other side, the comparison with BIRA-IASB CTM MAGRITTE/TM5 columns also give confidence into the physical soundness of the measurements. Although there are obviously some larger differences in the absolute column numbers, the seasonal variations are very consistent, even in strongly polluted regions like China.

7. References

Alvarado, L. M. A., Richter, A., Vrekoussis, M., Hilboll, A., Kalisz Hedegaard, A. B., Schneising, O., and Burrows, J. P.: Unexpected long-range transport of glyoxal and formaldehyde observed from the Copernicus Sentinel-5 Precursor satellite during the 2018 Canadian wildfires, *Atmos. Chem. Phys.*, 20, 2057–2072, <https://doi.org/10.5194/acp-20-2057-2020>, 2020.

Alvarado, L. M. A., Richter, A., Vrekoussis, M., Wittrock, F., Hilboll, A., Schreier, S. F. and Burrows, J. P.: An improved glyoxal retrieval from OMI measurements, *Atmos. Meas. Tech.*, 7(12), 4133–4150, doi:10.5194/amt-7-4133-2014, 2014.

Bauwens, M., Stavrou, T., Müller, J.-F., De Smedt, I., Van Roozendaal, M., van der Werf, G. R., Wiedinmyer, C., Kaiser, J. W., Sindelarova, K. and Guenther, A.: Nine years of global hydrocarbon emissions based on source inversion of OMI formaldehyde observations, *Atmos. Chem. Phys.*, 16(15), 10133–10158, doi:10.5194/acp-16-10133-2016, 2016.

Chan Miller, C., Gonzalez Abad, G., Wang, H., Liu, X., Kurosu, T., Jacob, D. J. and Chance, K.: Glyoxal retrieval from the Ozone Monitoring Instrument, *Atmos. Meas. Tech.*, 7(11), 3891–3907, doi:10.5194/amt-7-3891-2014, 2014.

Irie, H., Takashima, H., Kanaya, Y., Boersma, K. F., Gast, L., Wittrock, F., Brunner, D., Zhou, Y. and Van Roozendaal, M.: Eight-component retrievals from ground-based MAX-DOAS observations. *Atmospheric Measurement Techniques*, 4, 1027–1044, 2011.

Javed, Z., Liu, C., Khokhar, M., Tan, W., Liu, H., Xing, C., Ji, X., Tanvir, A., Hong, Q., Sandhu, O., Rehman, A., Javed, Z., Liu, C., Khokhar, M. F., Tan, W., Liu, H., Xing, C., Ji, X., Tanvir, A., Hong, Q., Sandhu, O. and Rehman, A.: Ground-Based MAX-DOAS Observations of CHOCHO and HCHO in Beijing and Baoding, China, *Remote Sens.*, 11(13), 1524, doi:10.3390/rs11131524, 2019.

Müller, J.-F. and Brasseur, G.: IMAGES: A three-dimensional chemical transport model of the global troposphere, *J. Geophys. Res.*, 100(D8), 16445, doi:10.1029/94JD03254, 1995.

Myriokefalitakis, S., Daskalakis, N., Gkouvousis, A., Hilboll, A., van Noije, T., Williams, J. E., Le Sager, P., Huijnen, V., Houweling, S., Bergman, T., Nüß, J. R., Vrekoussis, M., Kanakidou, M., and Krol, M. C.: Description and evaluation of a detailed gas-phase chemistry scheme in the TM5-MP global chemistry transport model (r112), *Geosci. Model Dev.*, 13, 5507–5548, <https://doi.org/10.5194/gmd-13-5507-2020>, 2020.

Lerot, C., Stavrou, T., De Smedt, I., Müller, J.-F. and Van Roozendaal, M.: Glyoxal vertical columns from GOME-2 backscattered light measurements and comparisons with a global model, *Atmos. Chem. Phys.*, 10(24), 12059–12072, doi:10.5194/acp-10-12059-2010, 2010.

Rothman, L. S., Gordon, I. E., Babikov, Y., Barbe, A., Chris Benner, D., Bernath, P. F., Birk, M., Bizzocchi, L., Boudon, V., Brown, L. R., Campargue, A., Chance, K., Cohen, E. A., Coudert, L. H., Devi, V. M., Drouin, B. J., Fayt, A., Flaud, J.-M., Gamache, R. R., Harrison, J. J., Hartmann, J.-M., Hill, C., Hodges, J. T., Jacquemart, D., Jolly, A., Lamouroux, J., Le Roy, R. J., Li, G., Long, D. A., Lyulin, O. M., Mackie, C. J., Massie, S. T., Mikhailenko, S., Müller, H. S. P., Naumenko, O. V., Nikitin, A. V., Orphal, J., Perevalov, V., Perrin, A., Polovtseva, E. R., Richard, C., Smith, M. A. H., Starikova, E., Sung, K., Tashkun, S., Tennyson, J., Toon, G. C., Tyuterev, V. I. G. and Wagner, G.: The HITRAN2012 molecular spectroscopic database, *Journal of Quantitative Spectroscopy and Radiative Transfer*, 130, 4–50, doi:10.1016/j.jqsrt.2013.07.002, 2013.

Serdyuchenko, A., Gorshchev, V., Weber, M., Chehade, W. and Burrows, J. P.: High spectral resolution ozone absorption cross-sections – Part 2: Temperature dependence, *atmospheric Measurement Techniques*, 7(2), 625–636, doi:<https://doi.org/10.5194/amt-7-625-2014>, 2014.

Sinreich, R., Volkamer, R., Filsinger, F., Frieß, U., Kern, C., Platt, U., Sebastián, O. and Wagner, T.: MAX-DOAS detection of glyoxal during ICARTT 2004, *Atmos. Chem. Phys.*, 7(5), 1293–1303, doi:10.5194/acp-7-1293-2007, 2007.

Sinreich, R., Coburn, S., Dix, B. and Volkamer, R.: Ship-based detection of glyoxal over the remote tropical Pacific Ocean, *Atmos. Chem. Phys.*, 10(23), 11359–11371, doi:10.5194/acp-10-11359-2010, 2010.

Stavrakou, T., Müller, J.-F., Bauwens, M., Smedt, I. De, Lerot, C., Roozendael, M. Van, Coheur, P.-F., Clerbaux, C., Boersma, K. F., A. R. van der, Song, Y., Jeong, S.-J., Huang, X., Song, Y., Li, M., Li, J., Zhu, T., Yamaji, K., Werf, G. R. van der, Huang, X., Li, M., Li, J., Song, Y., Fu, T.-M., Levelt, P. F., Smedt, I. De, Smedt, I. De, Boersma, K. F., Lerot, C., Müller, J.-F., Stavrakou, T., Stavrakou, T., Müller, J.-F., Smedt, I. De, Roozendael, M. Van, Werf, G. van der, Giglio, L., Guenther, A., Stavrakou, T., Guenther, A., Karl, T., Harley, P., Wiedinmyer, C., Palmer, P. I., Geron, C., Li, M., Andreae, M. O., Merlet, P., Akagi, S., Kurokawa, J., Sun, L., Jin, X., Holloway, T., Safieddine, S., Chaudhry, Z., Shi, Z., Tao, J. Z., Wang, Z., Han, D., Li, S., Su, L., Chen, L., Deng, X., Dee, D. P., Randerson, J., Chen, Y., Werf, G., Rogers, B., Morton, D., Kaiser, J., Wiedinmyer, C., Kudo, S., Inomata, S., Warneke, C., Yokelson, R. J., Korontzi, S., McCarty, J., Loboda, T., Kumar, S., Justice, C., Fu, T.-M., Stavrakou, T., Castellanos, P., Boersma, K. F., Werf, G. R. van der, Razavi, A., Stavrakou, T., Lin, J., Castellanos, P., Boersma, K. F., Torres, O., Haan, J. F. de, Barkley, M. P., Roberts, G., Wooster, M. J., Lagoudakis, E., Stavrakou, T., Miller, C. C., Jacob, D. J., et al.: Substantial Underestimation of Post-Harvest Burning Emissions in the North China Plain Revealed by Multi-Species Space Observations, *Sci. Reports*, Publ. online 31 August 2016; | doi:10.1038/srep32307, 6, 615–619, doi:10.1038/SREP32307, 2016.

Thalman, R., Baeza-Romero, M. T., Ball, S. M., Borrás, E., Daniels, M. J. S., Goodall, I. C. A., Henry, S. B., Karl, T., Keutsch, F. N., Kim, S., Mak, J., Monks, P. S., Muñoz, A., Orlando, J., Peppe, S., Rickard, A. R., Ródenas, M., Sánchez, P., Seco, R., Su, L., Tyndall,

G., Vázquez, M., Vera, T., Waxman, E. and Volkamer, R.: Instrument intercomparison of glyoxal, methyl glyoxal and NO₂ under simulated atmospheric conditions, *Atmos. Meas. Tech.*, 8(4), 1835–1862, doi:10.5194/amt-8-1835-2015, 2015.

Valks, P., Hao, N. and Lerot, C.: Algorithm Theoretical Basis Document for GOME-2 glyoxal column data records, SAF/AC/DLR/ATBD/GLY/01; Iss. 1/B., 2020.

Vandaele, A. C., Hermans, C., Simon, P. C., Carleer, M., Colin, R., Fally, S., Mérienne, M. F., Jenouvrier, A. and Coquart, B.: Measurements of the NO₂ absorption cross-section from 42000 cm⁻¹ to 10000 cm⁻¹ (238-1000 nm) at 220 K and 294 K, *Journal of Quantitative Spectroscopy and Radiative Transfer*, 59(3–5), 171–184, doi:10.1016/S0022-4073(97)00168-4, 1998.

Vlemmix, T., Piters, A. J. M., Berkhout, A. J. C., Gast, L. F. L., Wang, P., and Levelt, P. F.: Ability of the MAX-DOAS method to derive profile information for NO₂: can the boundary layer and free troposphere be separated?, *Atmos. Meas. Tech.*, 4, 2659–2684, doi:10.5194/amt-4-2659-2011, 2011

Volkamer, R., Spietz, P., Burrows, J. and Platt, U.: High-resolution absorption cross-section of glyoxal in the UV–vis and IR spectral ranges, *Journal of Photochemistry and Photobiology A: Chemistry*, 172(1), 35–46, doi:10.1016/j.jphotochem.2004.11.011, 2005.

Vountas, M., Rozanov, V. V. and Burrows, J. P.: Ring effect: Impact of rotational Raman scattering on radiative transfer in earth's atmosphere, *Journal of Quantitative Spectroscopy and Radiative Transfer*, 60(6), 943–961, doi:10.1016/S0022-4073(97)00186-6, 1998.